Title

The enhancer RNA, AANCR, regulates APOE expression in astrocytes and microglia.

Journal

Nucleic Acids Research, 52(17)

Authors

Wan, Ma

Liu, Yaojuan

Li, Dongjun

et al.

Publication Date

2024-09-23

DOI

10.1093/nar/gkae696

Peer reviewed

Nucleic Acids Research, 2024, **52**, 10235–10254
https://doi.org/10.1093/nar/gkae696
Advance access publication date: 20 August 2024
Gene regulation, Chromatin and Epigenetics

The enhancer RNA, AANCR, regulates APOE expression in astrocytes and microglia

Ma Wan[1,†], Yaojuan Liu[2,†], Dongjun Li[2], Ryan J. Snyder[1], Lillian B. Elkin[1], Christopher R. Day[1], Joseph Rodriguez[1], Christopher Grunseich[3], Robert W. Mahley[4,5], Jason A. Watts[1,*] and Vivian G. Cheung[2,*]

[1]Epigenetics and Stem Cell Laboratory, National Institute of Environmental Health Sciences, National Institutes of Health, Research Triangle Park, NC 27709, USA
[2]Department of Pediatrics, University of Michigan, Ann Arbor, MI 48109, USA
[3]National Institute of Neurological Disorders and Stroke, National Institutes of Health, Bethesda, MD 20892, USA
[4]Gladstone Institute of Neurological Disease, San Francisco, CA, USA
[5]Department of Pathology and Medicine, University of California, San Francisco, CA, USA

[*]To whom correspondence should be addressed. Tel: +1 734 615 4999; Email: vgcheung@med.umich.edu
Correspondence may also be addressed to Jason A. Watts. Email: jason.watts@nih.gov
[†]The first two authors should be regarded as Joint First Authors.

Abstract

Enhancers, critical regulatory elements within the human genome, are often transcribed into enhancer RNAs. The dysregulation of enhancers leads to diseases collectively termed enhanceropathies. While it is known that enhancers play a role in diseases by regulating gene expression, the specific mechanisms by which individual enhancers cause diseases are not well understood. Studies of individual enhancers are needed to fill this gap. This study delves into the role of APOE-activating noncoding RNA, AANCR, in the central nervous system, elucidating its function as a genetic modifier in Alzheimer's Disease. We employed RNA interference, RNaseH-mediated degradation, and single-molecule RNA fluorescence *in situ* hybridization to demonstrate that mere transcription of AANCR is insufficient; rather, its transcripts are crucial for promoting *APOE* expression. Our findings revealed that AANCR is induced by ATM-mediated ERK phosphorylation and subsequent AP-1 transcription factor activation. Once activated, AANCR enhances *APOE* expression, which in turn imparts an inflammatory phenotype to astrocytes. These findings demonstrate that AANCR is a key enhancer RNA in some cell types within the nervous system, pivotal for regulating *APOE* expression and influencing inflammatory responses, underscoring its potential as a therapeutic target in neurodegenerative diseases.

Graphical abstract

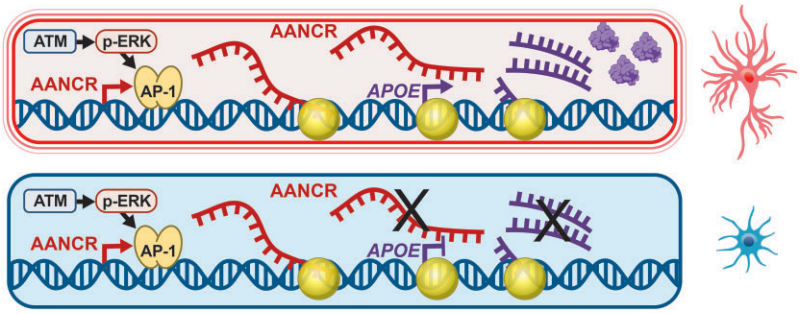

Introduction

Enhancer RNAs (eRNAs) as key regulators of gene expression are transcribed from noncoding DNA that makes up over 90% of the human genome. Enhancers orchestrate complex gene expression patterns essential for cellular functions. Large-scale screens have uncovered hundreds of thousands of enhancers that significantly influence gene expression, revealing their complex and varied nature (1–3). Through chromatin loops, most enhancers regulate gene expression in *cis* by interacting with neighboring genes. Enhancers are located upstream, downstream, and even within their target genes. Given their regulatory significance, it is not surprising that sequence variants within enhancers can affect their functions and therefore influence susceptibility to human diseases (4,5).

Transcription factors and RNA Polymerase II bind to a significant number of enhancers leading to the synthesis of enhancer RNAs (4,6–8). The locus control region of β-globin was among the first enhancers found to be transcribed (9). We now know that enhancer RNAs are common and they are essential parts of gene regulatory networks (7,10).

Many enhancer RNAs are not polyadenylated and are less stable than mRNAs thus their expression levels are usually

Received: May 1, 2024. **Revised:** July 26, 2024. **Editorial Decision:** July 27, 2024. **Accepted:** August 1, 2024
Published by Oxford University Press on behalf of Nucleic Acids Research 2024.

low. Their transient nature allows them to fine-tune gene expression during development and in stress responses. However, given their low and often brief expression, enhancer RNAs are less amenable to analysis. While we know the general features of enhancer RNAs as a class of nucleic acids, significant gaps remain in our understanding of most of them. For many enhancer RNAs, we do not know how they are controlled and the biological effects of their regulation of target genes are yet to be determined (11).

To gain a deeper understanding of gene regulation, it is essential to shift focus from examining enhancer RNAs collectively to investigating individual eRNAs in detail. The study of specific enhancer RNAs is vital for unraveling the complexities of gene regulatory mechanisms, and understanding how dysregulation leads to diseases. For example, studies that identified CCAT1 as an enhancer RNA that modulates *MYC* expression have deepened insights into long-range gene regulation (11,12). Similarly, research on HOTAIR has expanded our understanding of chromatin dynamics in cancer contexts (13,14). Additionally, investigations into the long-range enhancer affecting Sonic hedgehog have clarified the genetic underpinnings of polydactyly and enhanced our knowledge of limb bud development (15).

Previously, we identified an enhancer RNA, *APOE*-activating noncoding RNA, AANCR that influences the expression of *APOE*, a gene significantly associated with Alzheimer's Disease (16). We found that AANCR has characteristic features of enhancer RNAs. It is a capped, non-polyadenylated RNA. It is transcribed from a region on chromosome 19 between *TOMM40* and *APOE* characterized by DNaseI hypersensitivity and enhancer chromatin marks such as H3K27ac and H3K4me1. Like other enhancer RNAs, the expression level of AANCR is modest. Yet, we were able to uncover and study AANCR by using PROseq which enriches nascent RNA for sequencing (17).

AANCR expression varies by cell type as its transcription is regulated by RNA sequence and structure (16). In hepatocytes, the full-length AANCR is synthesized, and it enhances the expression of *APOE*. In other cells such as B-cells and fibroblasts, AANCR is only partially transcribed because RNA Polymerase II elongation is obstructed by R-loops, which are stabilized through sequential RNA modifications where adenosines are N6-methylated and then cleaved leading to abasic sites. Under stress conditions, the nascent RNA of AANCR does not undergo these chemical modifications, therefore full-length AANCR is synthesized and in turn facilitates the expression of *APOE* in B-cells and other peripheral cells, which typically do not express *APOE* at baseline (16).

In this study, we advanced beyond the identification of AANCR to identify how it is regulated, and the biological consequences of its regulation of *APOE*. Given that sequence variants in AANCR are associated with Alzheimer's disease (16), we carried out these characterizations using cells from the nervous system. We uncovered that, unlike some eRNAs where transcription alone is sufficient for function, AANCR requires its transcripts to regulate *APOE* expression at baseline and in stress responses. We found an ATM-mediated mechanism that activates AANCR in mitochondrial stress response. Then in gene expression and mitochondrial function analyses, we found that AANCR and *APOE* confer an inflammatory phenotype to astrocytes. This study adds to our knowledge of enhancer RNAs by identifying that AANCR's transcripts are necessary for regulation and elucidating the AANCR regulatory network, including its upstream regulators and the broader downstream consequences of AANCR-regulated *APOE* expression.

Methods (see Resource Table in supplemental material for manufacturers and catalog numbers)

AANCR, APOE genomic location (hg38): chr19:44903728–44905635 for AANCR, chr19:44905796–44909393 for APOE, Supplementary Figure S1.

APOE quantitation (secreted protein)

To quantify the secreted APOE protein, cells were serum starved for 24 h, and the medium from each sample was collected and concentrated ten times with Protein Concentrator PES, 10K molecular weight cut-off. Concentrated medium was mixed 1:1 in 2× sample loading buffer and run on SDS PAGE gel. Following membrane transfer Western blot was performed using APOE antibody (Sigma).

Antisense oligonucleotides against AANCR in astrocytes and microglia

Cells were grown to a confluence of 50% in T-25 flasks or 6-well plates. The AANCR GapmeR was transfected at 10 nM using Lipofectamine 3000 in astrocytes or microglia. Four days post-transfection cells were washed in PBS and collected by cell scraping for downstream analysis.

Aβ aggregates in microglia, B-cells, and astrocytes

For the preparation of amyloid beta protein fragment 42 (Aβ42) or amyloid beta protein fragment 40 (Aβ40): Briefly, Aβ42 or Aβ40 were dissolved in dimethyl sulfoxide (DMSO) to a stock concentration of 5 mM, and then diluted in water to make 100 μM working stock solutions which were incubated for 5 days at 37°C. For treatment, the cells were washed twice with PBS and placed in serum-free media. Twenty-four hours later, Aβ42 or Aβ40 were added to the cells at a final concentration of 10 μM in the media and the cells were treated for 30 h (B-cells) or 54 h (astrocytes and microglia).

Antimycin A in microglia, astrocytes and B-cells

Antimycin A was dissolved in dimethyl sulfoxide (DMSO) and further diluted in sterile culture medium immediately before use. Antimycin A (or equal volume of DMSO) was added to the cell culture medium to a final concentration of 10 μM and cells were maintained for the indicated treatment duration. For adherent cells, the culture media was retained for analysis of secreted APOE, and the cells were processed for gene expression or protein analysis as described below. B-cells were pelleted by centrifugation, washed with PBS and cells were processed for downstream analysis.

cDNA-seq

From astrocytes transfected with siRNA against AANCR or/and APOE or non-target siRNA, sequencing libraries were prepared using TruSeq Stranded Total RNA Library Prep Kit (Illumina). Sequencing was performed on NovaSeq6000 and >150 million 100-nt paired-end reads were generated from each sample. Sequencing reads were aligned to the GRCh38 (hg38) human reference sequence using GSNAP

(v. 2021-12-17) (18) with one mismatch allowed, and soft-clipping on. Over 75% of the reads were uniquely aligned (average = 75% (siAANCR samples), 84% (siAPOE samples). Gene expression levels were quantified using Cufflinks v.2.2.1 (19). The distributions of the expression levels were highly similar across samples ($P > 0.1$, *t*-test). In all the AANCR and APOE knockdown samples as well as those treated with siRNAs with scrambled sequences (or non-target controls, NTC), we identified expressed genes as those with expression levels across the knockdown samples and controls of FPKM ≥ 2. In the AANCR knockdown experiments, there were five siAANCR samples and NTC controls, for each gene, we summed the expression levels across those samples, if the summed FPKM >2, then it is included in the analysis as expressed. The same analysis was carried out for the siAPOE experiments. This expression level cutoff gave us ∼12 000 expressed genes in the siAANCR and siAPOE experiments.

As an independent measure of differential gene expression, we obtained the raw read counts for the ∼12 000 expressed genes using Rsubread version 2.14.2 and compared between the siRNA and NTC samples using DESeq2 version 1.42.1 under default settings (20).

We compared the *P*-values from the *t*-test and DESeq2 analyses. The results are highly similar. For the 598 significant genes, we compared the *P*-values from the *t*-test and DESeq2 and found a Jaccard Index of 0.76 and a Dice coefficient of 0.865. Comparing the *P*-values of all expressed genes, we found a Spearman Rank Correlation with a *P*-value $<<10^{-10}$, a Szymkiewicz–Simpson coefficient of 0.74, and a kappa statistic of 0.60 for the significance classification.

Cell culture

Human lymphoblastoid B-cells from controls and patients with Ataxia Telangiectasia (AT) were grown in Roswell Park Memorial Institute media, RPMI 1640, supplemented with 15% fetal bovine serum, 100 U/ml penicillin/100 μg/ml streptomycin, and 2 mmol/l L-glutamine. HEK 293T cells were maintained in Dulbecco's modified Eagle's medium (DMEM) with 10% FBS, 1% GlutaMAX and 100 U/ml penicillin/100 μg/ml streptomycin. HK-2 cells were maintained in DMEM-F12 media supplemented with 10% FBS and 100 U/ml penicillin/100 μg/ml streptomycin. Primary human astrocytes were seeded on poly-L-lysine-coated (2 μg/cm^2) T-75 culture flasks with complete astrocyte medium. The medium was changed every three days, until cells were approximately 70% confluent and then changed daily until the cell confluence reached 90% confluence. Astrocytes were passaged when cells reached 90–95% confluency. Human microglia were grown in DMEM supplemented with 10% fetal bovine serum, 100 U/ml penicillin and 100 μg/ml streptomycin. All cells were grown at 37°C, 5% CO_2. Adherent cells were passaged every 72 h using trypsin–EDTA 0.025% for astrocytes and 0.05% for the other cell lines.

Chromatin immunoprecipitation

Two independent CRISPR edited cell lines where the AP-1 site was mutated and two cell lines where the AP-1 site was not edited, were used for ChIP following the protocol described (21). Briefly, cells were cross-linked with 1% formaldehyde for 10 min followed by neutralization with 2.5M glycine for 5 min. For nuclei isolation, crosslinked cells were rotated for 10 min at 4°C in 5 ml lysis buffer 1 (50 mM HEPES pH 7.6, 140 mM NaCl, 1 mM EDTA, 10% glycerol, 0.5% Igepal CA-630, 0.25% Triton X-100) followed by pelleting, and a 10 min rotation in 5 ml lysis buffer 2 (200 mM NaCl, 1 mM EDTA, 0.5 mM EGTA, 10 mM Tris, pH 8). Nuclei were pelleted followed by swelling in lysis buffer 3 (10 mM Tris, pH 8, 1 mM EDTA, 0.5 mM EGTA, 100 mM NaCl, 0.1% deoxycholic acid, 1% *N*-lauryl sarcosine) for 10 min, then sonicated on high setting (30 s on, 30 s off) for 15 min to shear chromatin to <500 bp with Bioruptor. 50 μg sheared chromatin for each sample was incubated in RIPA buffer (50 mM Tris, pH8, 150 mM NaCl, 1% NP-40, 0.5% sodium deoxycholate, 0.1% SDS) with 5 μg antibody against Jun or IgG. Target chromatin fragments were recovered with Protein G beads. Beads were washed twice with low salt RIPA (150 mM NaCl) and twice in high salt RIPA (300 mM NaCl), then eluted in 100 μl 1% SDS plus 100 mM sodium bicarbonate. After cross-link reversal, DNA was purified with a QIAquick PCR Purification Kit and quantified by qPCR using primers listed in the Resource Table.

Cortical neuron differentiation from human iPSCs

Differentiation was performed as previously described (22). In brief, stably transfected control iPSCs with the NGN2 cassette were plated at 30 000 cells/cm^2 on a matrigel coated surface in E8 Flex medium containing 10 μM ROCK inhibitor. 24 h later, cells were induced with Neural Induction Medium (NIM): DMEM/F12, B27(1×), N2 (1×), NEAA (1×), GlutaMax (1×), ROCK inhibitor (10 μM), and doxycycline 2 μg/ml. After 48 h of doxycycline treatment, cortical neurons were dissociated with accutase to single cells and re-plated at 50 000 cells/cm^2 on Matrigel coated surfaces in Neural Maintenance Medium (NMM): DMEM/F12:Neurobasal medium, B27 (1×), N2 (1×), NEAA (1×), GlutaMax (1×), doxycycline (2 μg/ml), laminin (1 μg/ml), BDNF (10 ng/ml), NT3 (10 ng/ml). On day 4, cells were transfected with siRNA for AANCR and non-targeting control at final concentrations of 20 nM using RNAiMax. Cells were collected 72 h post transfection and total RNA was extracted using TRIzol and chloroform and purified with a RNeasy Kit following the manufacturer's instructions.

CRISPR-mediated editing

sgRNA sequence to target the AP-1 site at AANCR locus was selected using CRISPR Targets tool in UCSC genome browser (https://genome.ucsc.edu). sgRNA oligos were annealed and phosphorylated (see Resource Table) followed by cloning into plasmid pSpCas9(BB)-2A-GFP (PX458), a gift from Feng Zhang (Addgene plasmid # 48138) (23). The 100-nucleotide single-stranded DNA oligonucleotide (ssODN) repair template (see Resource Table) was centered at the predicted CRISPR/Cas9 cleavage site and designed to introduce three point-mutations in the putative AP-1 binding site and prevent recutting after gap repair. pSpCas9(BB)-2A-GFP with the sgRNA targeting AANCR was co-transfected with the ssODN into HEK 293T. Cells were plated at 2.5 × 10^5 per well in 12-well dishes and transfected with 500 ng pSpCas9(BB)-sgRNA-2A-GFP and 1 μl of 10μM ssODN template DNA using Lipofectamine LTX. Then 36–48 h after transfection, cells were well-disassociated and GFP-positive cells were FACS sorted into 96-well plates (one cell/well) pre-coated with gelatin and cultured for 2–3 weeks to allow for single colony growth. Following cell expansion, genomic DNA was isolated from single

colonies and editing was verified by PCR followed by Sanger sequencing.

Extracellular flux analysis

For Seahorse analysis (XFe24, Agilent Technologies), astrocytes were seeded at a density of 100 000 cells/well in poly-L-lysine-coated XFe24 cell culture microplates. Cells were transfected with siRNA against AANCR as described above, and after 48 h the astrocytes were washed twice with XF DMEM medium supplemented with 100 μM pyruvate, 200 μM L-glutamine and 1.1 μM glucose, and 0.5% serum, then allowed to incubate in supplemented XF DMEM for 1 h at 37°C and 0% CO_2. Cells were then tested for oxygen consumption rate (OCR) and extracellular acidification (ECAR) over a continuous 12-h period with measurements taken every 30 min. ECAR and OCR values were then normalized to cell counts in each well.

Gene annotation and network analyses

Network analysis was carried out using STRING (24), the edges indicate functional and physical interactions based on the strength of experimental, co-expression, databases and neighborhood evidence. K-means clustering implemented in STRING were performed. Interactions were further analyzed using Biogrid as implemented in NIA DAVID (25).

Immunoblots

Following treatment, cells were washed with ice-cold PBS and placed in RIPA buffer supplemented with Protease Inhibitor Cocktail, Phosphatase Inhibitor Cocktail 2 and Phosphatase Inhibitor Cocktail 3, and held on ice 10 min. Western blots were performed by running whole cell lysates on 4–12% Bis–Tris Protein Gels in 1× MES SDS running buffer. Proteins were transferred to PVDF membrane in 1× transfer buffer at 100V for 1 hour at 4°C. The membranes were blocked with 5% powdered milk in 1× TBST buffer. The primary antibodies for APOE, phospho-ATM, total ATM, phospho-ERK1/2, total ERK1/2, phospho-c-JUN, total c-JUN are listed in the Resource Table. Protein abundance was determined by chemiluminescence.

Jun inhibitor SP600125

Jun N-terminal kinase (JNK) inhibitor SP600125 was dissolved in dimethyl sulfoxide (DMSO) and further diluted in sterile culture medium immediately before use. SP600125 was added to the culture medium at 20 μM for 16 h alone and cells were collected for protein isolation and subsequent immunoblotting. To measure changes in gene expression, microglia cells were treated with SP600125 at 20 μM for 16 h followed by the addition of antimycin A (or vehicle) at 10 μM for 2 and 6 h.

Paraquat in astrocytes

Paraquat was dissolved to 100 mM in distilled water. Paraquat was added to the astrocyte cultures at doses of 100 μM and cells were treated for 72 h. Cells were collected for gene expression analysis as described below.

qPCR of AANCR and APOE

Following treatment, cells were washed with PBS and collected by cell scraping. Total RNA was isolated using the RNeasy Mini-Kit (Qiagen) and 0.5 μg RNA was converted to cDNA using Taqman RT kit using random hexamer priming. Gene expression was determined by quantitative PCR using SYBR Green PCR Master Mix on Applied Biosystem QuantStudio 5 Real-Time PCR System, and gene expression was normalized to GAPDH using the delta-Ct method. Sequences for the primers used are shown in the Resource Table.

siRNA knockdown of AANCR and APOE in astrocytes, microglia, and iPSC-neurons

Cells were seeded in 6-well plates or T-25 flasks until they reached 50–60% confluence and were transfected with siRNA using Lipofectamine RNAiMax to a final concentration of 5 nM for astrocytes, and 10 nM for microglia or iPSC-neurons. 24–48 h post-transfection cells were washed in PBS and collected by cell scraping for downstream gene expression analysis or for protein analysis. The siRNA targeting AANCR and APOE are listed in the Resource Table.

Single-molecule RNA fluorescence *in situ* hybridization (smFISH)

Astrocyte or HK-2 cells were grown on glass cover slips and 50 mM NaCl was added to the media to induce hypertonic stress. Cells were fixed using 4% PFA for 10 min at room temperature. Excess PFA was removed by washing with PBS and then the cells were permeabilized with 70% ethanol overnight at 4°C. FISH probes to AANCR (26 probes), *APOE* (29 probes) were designed with Stellaris Probe Designer (https://www.biosearchtech.com/stellaris-designer) and ordered with Quasar 570 (AANCR probes) or Quasar 670 (*APOE*) label. Probes were hybridized as previously described (26). Briefly, probe hybridization was carried out at 37°C following the adherent mammalian cell protocol from Biosearch Stellaris. Images were acquired and 900–1300 nuclei per sample were analyzed with RNA smFISH spots identified by fitting to a 2D Gaussian mask and performing local background subtraction as previously described (27). Nuclei with one or more spots where AANCR and *APOE* signals overlapped within 0.825μm were considered to have colocalization. We measured the average nuclear area to be 78.5 um^2 (astrocytes); there was one (median) AANCR transcript and seven (median) APOE transcripts per nucleus. The area of a smFISH spot is 1% of the nuclear area, so on average 1% of the nuclear area is occupied by AANCR and 7% is occupied by APOE, therefore 0.07% of nuclei will show colocalization by chance. The percentage of nuclei with colocalized AANCR and APOE spots are reported from at least two experiments. As negative controls, we used the smFISH data for *AGR2* and *TFF1* (26). The signal intensities and colocalizations were analyzed as with AANCR and APOE and reported for triplicate experiments.

SR11302 and TPA in astrocytes with/without hypertonic stress

For osmotic stress treatments, astrocyte cell medium was supplemented with 50 mM NaCl for 2 h. For AP-1 inhibition SR11302 was added at 2 μM or 5 μM for 24 h. For AP-1 agonist treatment, TPA was added at 10 ng/ml or 50 ng/ml for 30 min. For combination treatments, the cells were incubated with SR11302 for 22 h and exposed to hypertonic stress for 2 h, followed by TPA treatment for 30 min where indicated.

Results

AANCR, an enhancer RNA, regulates *APOE* expression in human astrocytes, microglia and neurons

AANCR transcription is cell-type specific; it is transcribed into full-length transcripts only in cells that express *APOE* (16). This suggests that AANCR transcripts are necessary to promote *APOE* expression, however, transcription alone may mediate accessible chromatin and therefore *APOE* expression. Here, in cells from the nervous system, we asked if AANCR transcripts are needed to regulate *APOE* expression.

In the brain, *APOE* is synthesized mostly by astrocytes, but the transcriptional regulation of *APOE* in astrocytes was unknown (28). We asked if AANCR regulates *APOE* expression in astrocytes and whether the transcripts of AANCR are needed for gene regulation. We began by using RNA interference in astrocytes, to knock down AANCR transcripts with different siRNAs individually and as a pool. The results showed that RNA interference reduced the AANCR transcript level by about 50% (Figure 1A, $P < 0.005$, *t*-test); in the same cells, *APOE* expression also decreased significantly by about 50% (Figure 1B, $P < 0.005$, t-test). This suggests that in astrocytes AANCR regulates *APOE* expression and the AANCR transcripts are needed to facilitate the regulation. To ensure that the AANCR transcripts are indeed needed for regulation, we carried out RNaseH-mediated degradation of AANCR transcripts with a single-stranded DNA oligonucleotide specific to AANCR. The results showed that the antisense oligonucleotides (ASO) decreased AANCR transcript levels by more than 50% ($P < 0.05$, Figure 1C), and correspondingly *APOE* expression was significantly reduced ($P < 0.005$, Figure 1D). Given that APOE is a secreted protein, we measured the amount of APOE protein in the media. Figure 1E showed that the knockdown of AANCR also decreased the amount of secreted APOE protein. Astrocytes with lower AANCR expression secreted about 40% less APOE proteins (Figure 1E, $P < 0.005$, *t*-test). Together these results show that the enhancer RNA, AANCR, influences the expression of *APOE* in astrocytes, and the transcripts of AANCR are needed for this regulation.

Like astrocytes, microglia express *APOE* but at a lower level. We asked if, in microglia, *APOE* expression is also regulated by AANCR. We again decreased AANCR transcript levels by RNA interference and found that *APOE* expression level decreased correspondingly (Figure 2A and B, $P < 0.005$, *t*-test). We also knocked down *APOE* by RNA interference, and while the expression level of *APOE* expression decreased ($P < 0.005$, Figure 2B), that of AANCR did not change (Figure 2A). To confirm this, we repeated the experiment in astrocytes, and the results also showed that knockdown of *APOE* reduced *APOE* expression but not AANCR expression levels (Supplementary Figure S2). AANCR is a noncoding RNA found upstream of *APOE,* this result shows that AANCR is an independent transcript that regulates *APOE*, and there is no apparent feedback loop where *APOE* regulates AANCR.

In iPSC-derived neurons, we again performed RNA interference experiments against AANCR. AANCR transcript level was significantly reduced, and correspondingly *APOE* expression was reduced significantly (Figure 2C, D). Together these results show that in different cell-types in the nervous system, AANCR regulates *APOE* expression through its transcripts.

AANCR co-localizes with APOE within single cells

The RNA interference and RNaseH-mediated degradation of AANCR transcripts were carried out in bulk cells. If AANCR transcripts are needed to mediate *APOE* expression, then as an enhancer RNA, AANCR transcripts should localize to the *APOE* gene locus. If so, it is likely that AANCR and *APOE* transcripts would colocalize within individual cells at the *APOE* locus. So next, we conducted single-cell analyses to assess this interaction and confirm that *APOE* is a direct target of AANCR.

We performed single-molecule RNA fluorescence hybridization (smFISH) to measure the association between AANCR and *APOE*. Previously, we found that *APOE* expression is induced in renal tubule cells following hypertonic stress (16). Here, we found that when renal tubule cells are exposed to hypertonic conditions, within 15 min, AANCR transcripts co-localized with *APOE* (Figure 3A) in about 40% of the nuclei ($P < 0.001$, t-test). Figure 3B showed a time-dependent increase in the number of nuclei where the transcripts of AANCR and *APOE* co-localized. We then asked if the same colocalization is found in astrocytes. At baseline, the transcripts of AANCR are co-localized with those of *APOE* in >10% of the nuclei, which is significantly ($P < 0.03$; *t*-test) higher than the 0.07% colocalization that is expected by chance (Supplementary Figure S3A–D). Within 1 h of exposure to hypertonic stress, there was a significant ($P < 0.005$, *t*-test) increase, with >40% of nuclei showing colocalization of AANCR and *APOE* transcripts (Figure 3C and D). These results provide additional evidence that AANCR regulates *APOE* expression at baseline and in stress response through the juxtaposition of AANCR with the *APOE* gene.

AANCR induces APOE expression in response to stress

Next, we delved into AANCR's regulation of *APOE* in stress responses. Oxidative stress that results from mitochondrial dysfunction is associated with neurodegenerative diseases including Alzheimer's disease (29,30). Since *APOE* is a major susceptibility gene of Alzheimer's disease, it is important to understand its regulation in response to oxidative stress in the central nervous system. We induced oxidative stress by inhibiting the mitochondrial electron transport chain. We treated microglia with antimycin A which inhibits complex III of the mitochondrial electron transport chain (31,32). Figure 4A shows that antimycin A leads to a significant increase in AANCR expression and correspondingly a 50% and significant ($P < 0.01$, *t*-test) increase in *APOE* expression level (Figure 4B). The APOE is then secreted; Figure 4C shows a time-dependent increase (>2-fold) of APOE protein abundance in the media. Previously, studies have shown that mitochondrial stress increases *APOE* expression in human leukemia cells and astrocytes (33), here in microglia, we showed that in response to the disruption of complex III of the mitochondrial electron transport chain, AANCR is induced and this results in *APOE* gene and protein induction.

We then checked if AANCR-*APOE* expression is induced by other stressors, such as amyloid beta (Aβ) aggregates. Aβ is a proteolytic product of amyloid precursor protein. Gamma secretase cleaves the C-terminus of amyloid precursor protein leading to Aβ42 (42 residues) and Aβ40 (40 residues). Aβ42 with two extra hydrophobic amino acids forms fibrils more efficiently, making it a major component of amy-

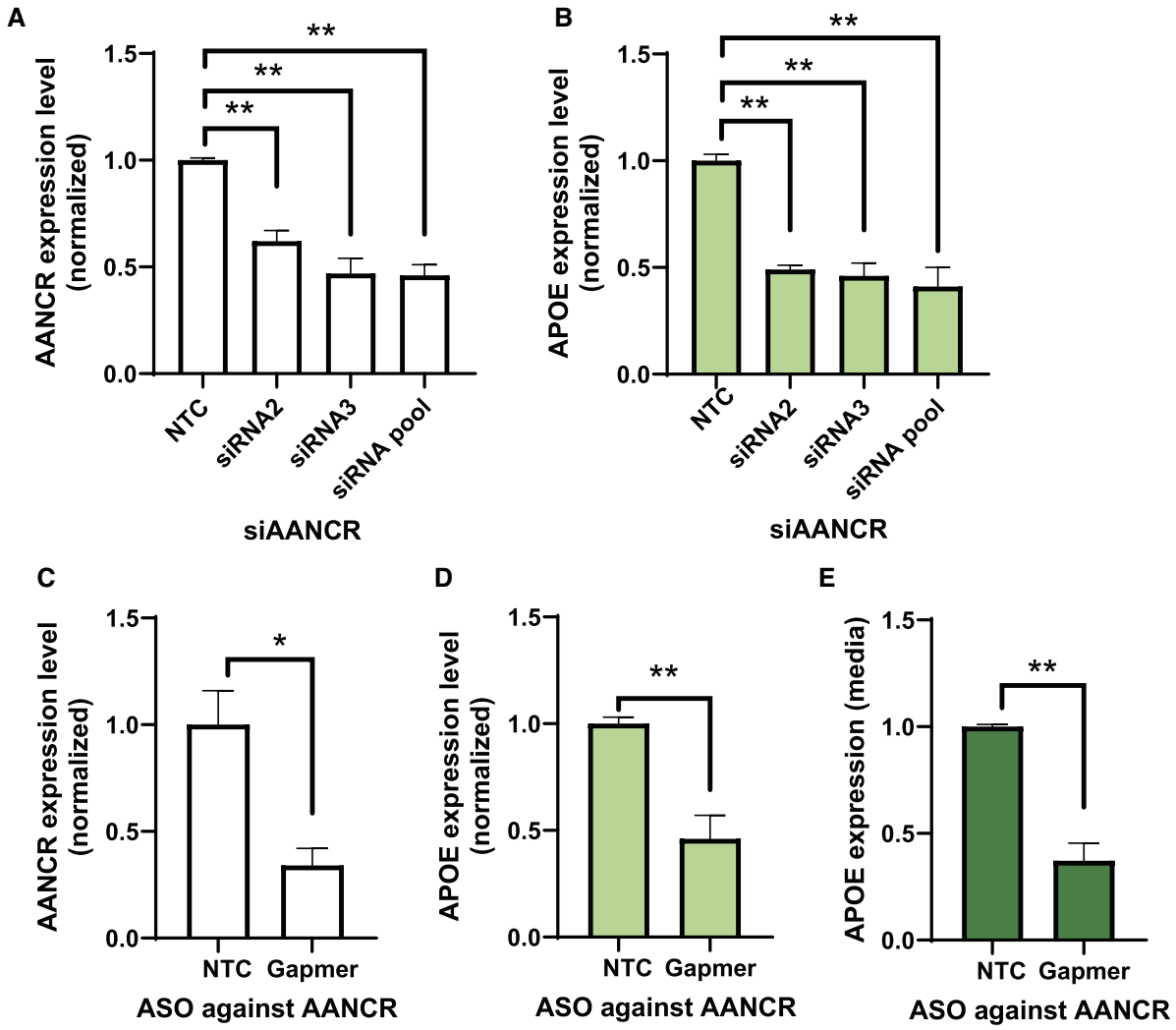

Figure 1. Knockdown of the enhancer RNA, AANCR, decreases *APOE* gene and protein expression in astrocytes. AANCR is knocked down by RNA interference with two separate siRNAs and as a pool of the two siRNAs. siRNA with scrambled sequence was used a control and labeled as nontarget control, NTC. The expression levels of AANCR (**A**) and *APOE* (**B**) decreased significantly after silencing the AANCR. AANCR expression decreased following knockdown with an antisense oligonucleotide (**C**), correspondingly the *APOE* expression decreased (**D**) and the amount of secreted APOE protein (**E**) was reduced significantly ($n \geq 3$, error bar = S.E.M. * $P < 0.05$, ** $P < 0.005$).

loid plaques. The accumulation of Aβ42 leads to oxidative stress (34–39). We incubated microglia with Aβ40 or Aβ42 aggregates. Figure 4D shows that amyloid beta aggregates with 42 amino acid residues significantly ($P < 0.001$, *t*-test) increased AANCR expression. Consequently, *APOE* expression also increased ($P < 0.05$, *t*-test Figure 4E). We repeated this experiment in human B-cells. The results showed that as in microglia, Aβ42 significantly increased AANCR and *APOE* expression in B-cells (Figure 4F and G). Thus, the expression response of AANCR and *APOE* to stress is similar in microglia, a cell type in the CNS and in peripheral B-cells.

We extended the study further into astrocytes to assess if another mitochondrial stressor, paraquat, also induces AANCR expression. Paraquat induces oxidative stress through increased free radical production. Results showed that paraquat significantly induced AANCR ($P < 0.01$, *t*-test) and *APOE* expression ($P < 0.05$, *t*-test) in astrocytes (Figure 5A and B). Similarly, Aβ42 induces AANCR and *APOE* expression in astrocytes (Figure 5C and D). It has been shown that Aβ42 induces *APOE* expression in astrocytes (40), here our results show that the induction is mediated by AANCR.

Together, we found that in human microglia, astrocytes and B-cells, various stresses induce AANCR and *APOE* expression further showing that AANCR regulates *APOE* expression in different cell types at baseline and in stress response.

AP-1 induces AANCR in response to stress

Since our goal is to study AANCR as an enhancer RNA in detail, next we investigated how AANCR transcription is induced. Data from the ENCODE project show that JUN and FOS transcription factors constituting the activator-protein 1, AP-1 (41–44), bind to the DNA that encodes AANCR, as shown in data from HepG2 cells (Figure 6A). We followed up the ENCODE data with chromatin immunoprecipitation which shows that JUN binds to the AP-1 site, and the binding is abrogated by mutation with CRISPR editing (Figure 6B).

To ask if the AP-1 site in the DNA that encodes AANCR regulates its expression in the CNS, we treated astrocytes with SR11302, a retinoid that specifically inhibits AP-1 (45). The

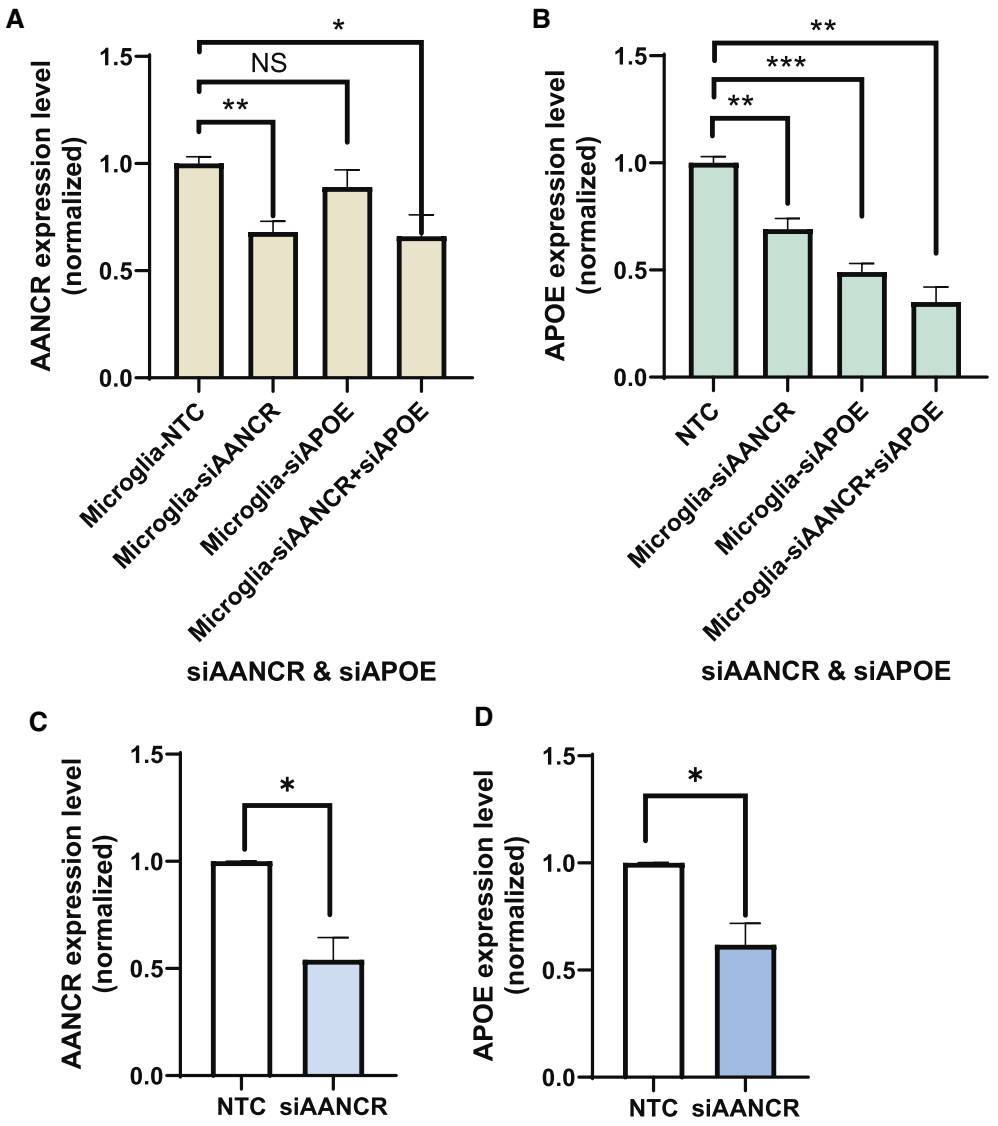

Figure 2. Knockdown of the enhancer RNA, AANCR, decreases *APOE* gene expression in microglia and iPSC-induced neurons. AANCR and *APOE* are knocked down with siAANCR (pool), si*APOE* (pool), and combined siAANCRs and si*APOE*s in microglia. The expression level of AANCR decreased significantly following AANCR but not after *APOE* silencing (**A**). *APOE* expression decreased after AANCR and *APOE* knockdowns as well as combined AANCR and *APOE* knockdown (**B**). The expression of AANCR decreased following siAANCR (pool) (**C**) and correspondingly *APOE* expression (**D**) also decreased significantly in iPSC-derived neurons ($n \geq 3$, error bar = S.E.M. NS = not significant, * $P < 0.05$, ** $P < 0.005$, ***$P < 0.001$).

results showed that upon inhibition of AP-1, AANCR expression decreased significantly ($P < 0.01$; *t*-test Figure 6C), and consequently *APOE* expression was reduced ($P < 0.05$, *t*-test Figure 6D). We then performed the opposite experiment and treated the astrocytes with 12–0-tetradecanoyl-phorbol-13- acetate (TPA), an activator of AP-1 (46), and measured the AANCR expression level. The results showed that TPA induced the expression of AANCR by almost 8-fold ($P < 0.001$; *t*-test Figure 6C) and the expression of *APOE* also increased correspondingly ($P < 0.01$; Figure 6D). SR11302 reduced AANCR expression to a lesser extent than the induction by TPA; to assess if this difference is due to the differential effect of SR11302 and TPA on AP-1 activity, we compared their activation of JUN. Supplementary Figure S4 shows that TPA induces JUN-phosphorylation faster (30 min versus 36 h) and to a greater extent (2.6-fold versus 1.5-fold) than SR11302.

Since SR11302 and TPA have a global effect, we also designed siRNA specific to the AP-1 site in AANCR and assessed its effects. In astrocytes, the knockdown of AANCR transcript with siAP-1 led to a reduction in AANCR expression and a corresponding decrease in *APOE* expression (Figure 6E).

To further explore the role of the AP-1 transcription factor complex in regulating AANCR during the stress response, we began by examining osmotic stress, as our previous research indicated that osmotic stress induces the transcription of both AANCR and *APOE*. We inhibited AP-1 in B-cells with SR11302 and exposed the cells to osmotic stress, the results showed that upon AP-1 inhibition, AANCR (Supplementary Figure S5A) and *APOE* (Supplementary Figure S5B) were induced at a significantly lower level in response to osmotic stress. The addition of TPA, an activator of AP-1, rescued the expression response of AANCR and *APOE*

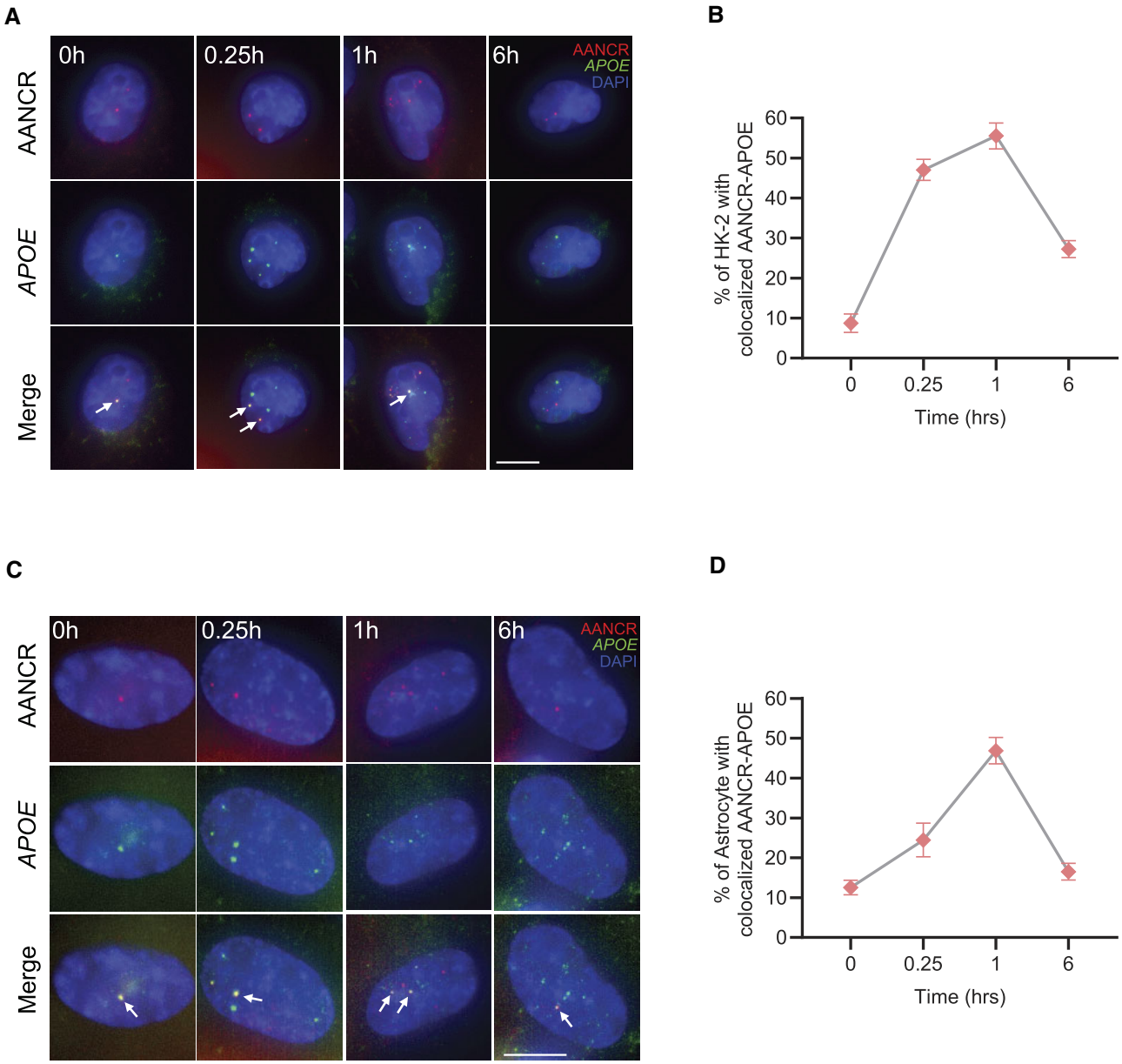

Figure 3. The co-localization of AANCR and *APOE* in single cells. Single-molecule RNA fluorescent *in situ* hybridization was carried out to assess the interaction of AANCR and *APOE* in the nuclei of single cells. Fluorescent smFISH images of AANCR (top, red) and *APOE* (middle, green) RNA in HK-2 proximal tubule cells at baseline (0 h) and following osmotic stress. In the merged images (bottom), arrows indicate AANCR-*APOE* colocalization (yellow). DAPI nuclear stain in blue. Scale bar 10 μm (**A**). Fraction of renal proximal tubule nuclei with AANCR-*APOE* colocation after osmotic stress is significantly higher ($P < 0.0001$; one-sided ANOVA; $n = 3$) after osmotic stress (**B**). Fluorescent smFISH images of AANCR (top, red) and *APOE* (middle, green) RNA in astrocytes at baseline (0 h) and following osmotic stress. In the merged images (bottom), arrows indicate AANCR-*APOE* colocalization (yellow). DAPI nuclear stain in blue. Scale bar 10 μm (**C**). Fraction of astrocyte nuclei with AANCR-*APOE* colocation after osmotic stress is significantly higher ($P < 0.001$; one-sided ANOVA; $n \geq 2$) after osmotic stress (**D**). In the experiments, 900–1300 nuclei were quantified per sample (error bar = S.E.M.).

(Supplementary Figure S4A and B) suggesting that in B-cells, AP-1 regulates AANCR transcription in stress response.

We then asked if AP-1 also regulates AANCR response to osmotic stress in astrocytes. Figure 6F and G show that in astrocytes, SR11302 inhibition of AP-1 leads to significantly lower AANCR and *APOE* expression levels at baseline and in response to stress. The effect of AP-1 inhibition on AANCR expression is stronger in response to stress, consistent with the role of AP-1 in stress response (18,19). Together, these findings suggest that AP-1 regulates AANCR and therefore *APOE* expression in various cell types at baseline and in response to stress.

ATM–ERK–AP1 pathway regulates AANCR

We then sought to identify the upstream pathway that activates AP-1 in AANCR to promote its transcription. Burg and colleagues have shown that Ataxia Telangiectasia Mutated (ATM), is a key signaling protein that mediates cellular response to osmotic stress (47). We asked if ATM is a signaling factor that influences AANCR and therefore *APOE* expression in response to osmotic stress. Using B-cells from five patients with Ataxia Telangiectasia (AT) due to ATM null mutations and B-cells from controls, we exposed the cells to osmotic stress and then measured AANCR and *APOE* expres-

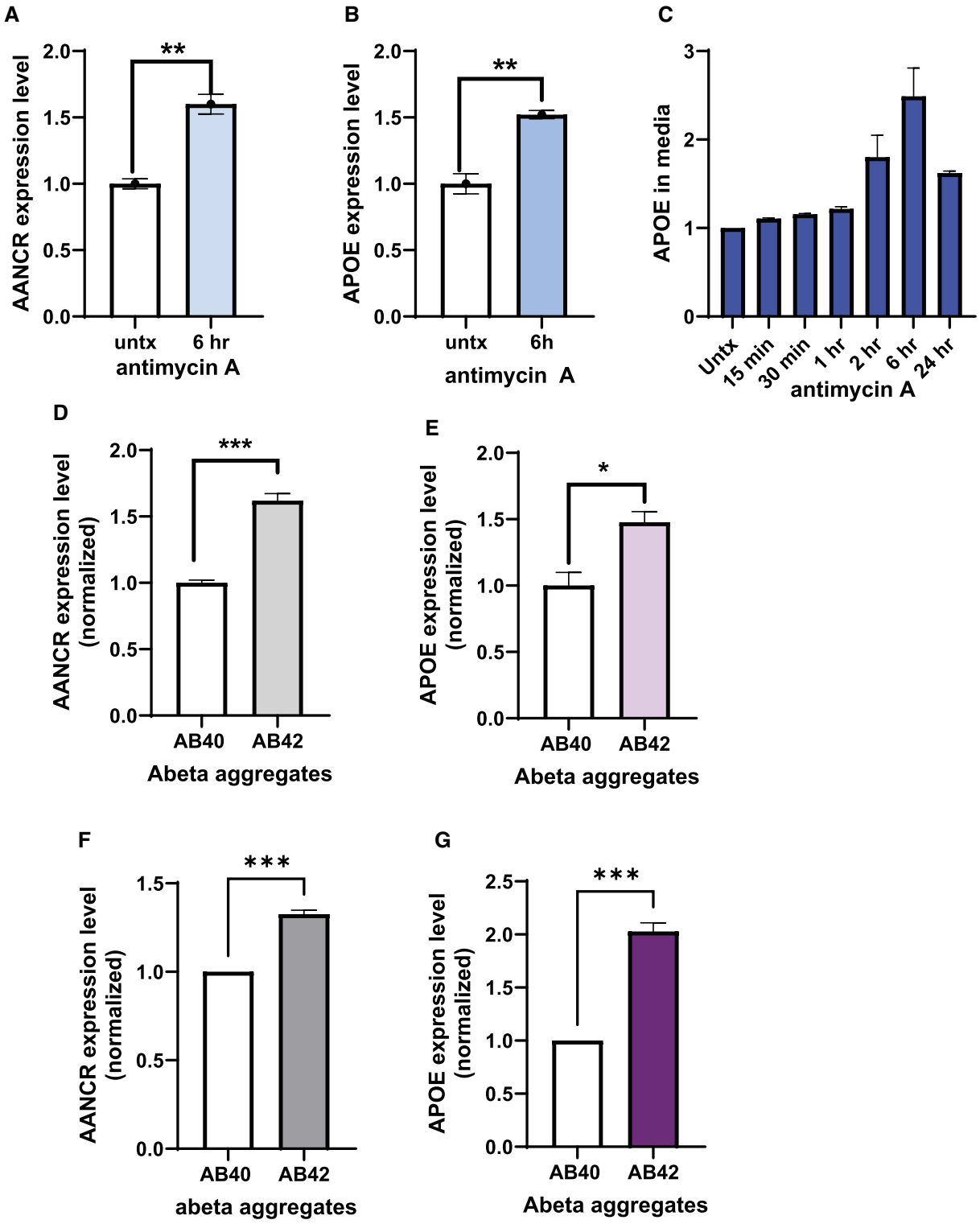

Figure 4. Antimycin A and Aβ42 aggregates induce AANCR and *APOE* expression in microglia and B-cells. In microglia treated with antimycin A, AANCR (**A**) and *APOE* (**B**) expression increased, and secreted APOE protein increased in a time-dependent manner (**C**). In microglia, AANCR (**D**) and *APOE* (**E**) expression levels increased in response to Aβ42 aggregates. In peripheral B-cells, AANCR (**F**) and *APOE* (**G**) expression levels also increased in response to Aβ42 aggregates ($n \geq 3$, error bar = S.E.M. * $P < 0.05$, ** $P < 0.005$, *** $P < 0.001$).

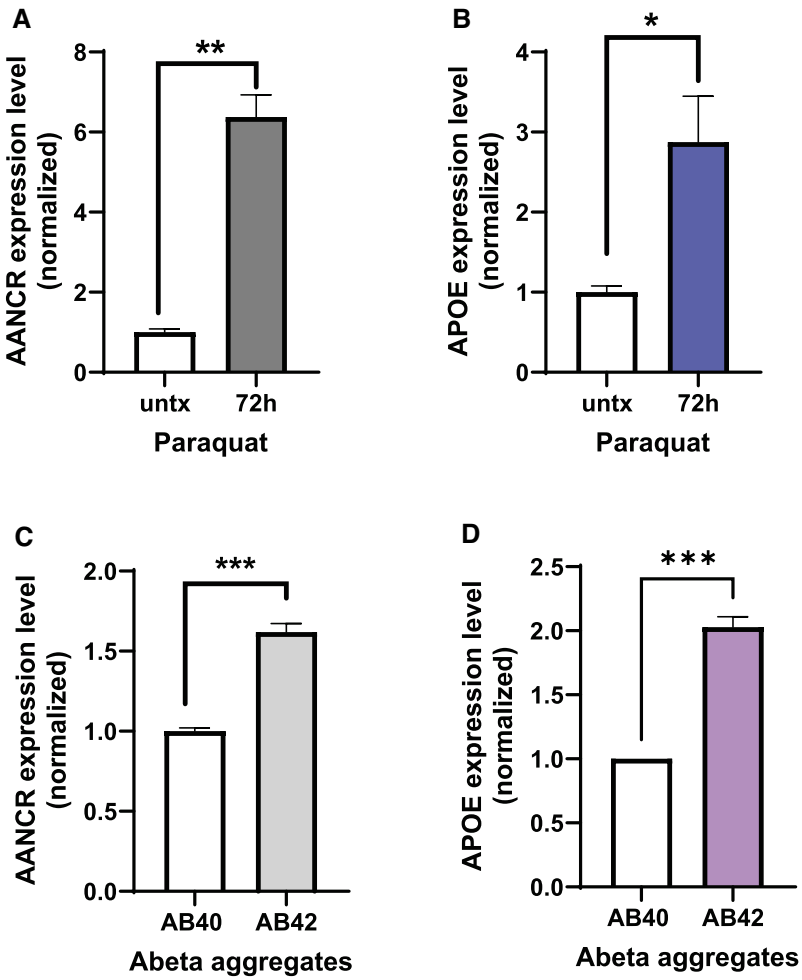

Figure 5. Paraquat and Aβ42 aggregates induce AANCR and *APOE* expression in astrocytes. In astrocytes, AANCR (**A**) and *APOE* (**B**) expression levels increased significantly following paraquat treatment. AANCR (**C**) and *APOE* (**D**) expression levels also increased in response to Aβ42 aggregates ($n \geq 3$, error bar = S.E.M. * $P < 0.05$, ** $P < 0.005$, ***$P < 0.001$).

sion. Figure 7A and B show that while AANCR and *APOE* expression were highly induced in the controls, they were only very modestly induced in the *ATM* null cells. Despite individual differences in AANCR and *APOE* stress-induced expression levels, the induction of AANCR ($P < 0.002$, *t*-test) and *APOE* ($P < 0.008$, *t*-test) expression levels are significantly higher in the control than the ATM null cells. This suggests that ATM is an upstream regulator of AANCR-*APOE*.

Next, we asked if ATM regulation of AANCR-*APOE* is specific to peripheral B-cells and osmotic stress, or if it is a general regulator of AANCR. To answer this question, we assessed the role of ATM in the induction of AANCR and *APOE* in microglia in response to mitochondrial stress. While we have B-cells from AT patients, we do not have microglia from AT patients. However, we could assess ATM activation when microglia are exposed to mitochondrial stress. We treated microglia with antimycin A as above (Figure 4) and assessed for ATM-phosphorylation. Figure 7C shows a representative immunoblot with antibodies against phospho-ATM. We found that ATM is phosphorylated in microglia within 15 mins (Figure 7C) of antimycin A treatment and the abundance of pATM continued to increase for 1 hour after antimycin. Our results are consistent with earlier findings by Tanya Paull and colleagues, that ATM is involved in oxidative stress response (48). Here, we extended Paull's salient results and found that in microglia, oxidative stress also activates ATM which then induces AANCR-*APOE* expression.

Next, we looked for regulatory proteins downstream of ATM that led to the activation of AP-1 in AANCR. We examined ERK, a kinase involved in oxidative stress responses including that induced by antimycin A (49–55). We treated microglia with antimycin A as above (Figure 4), and then measured pERK1/2. Results showed that after antimycin A treatment, ERK was activated ($P < 0.05$, *t*-test, Figure 7D) in about 20 min, and after the activation of ATM. This finding is consistent with the knowledge that ERK is a target of ATM (56,57).

Next, we examined the phosphorylation of JUN by treating microglia with antimycin A as above (Figure 4). We found that in the microglia, JUN was phosphorylated in a time-dependent fashion (Figure 7E) to a maximum level between 1 and 2 h ($P < 0.005$, ANOVA), which is after the activation of ATM and ERK. To confirm that JUN phosphorylation activates AANCR, we used a small molecule SP600125 to inhibit JUN phosphorylation (58). In microglia, we confirmed that SP600126 inhibited JUN phosphorylation, but not JUN expression (Figure 7F). We then treated the cells with SP600125 followed by antimycin A, and measured

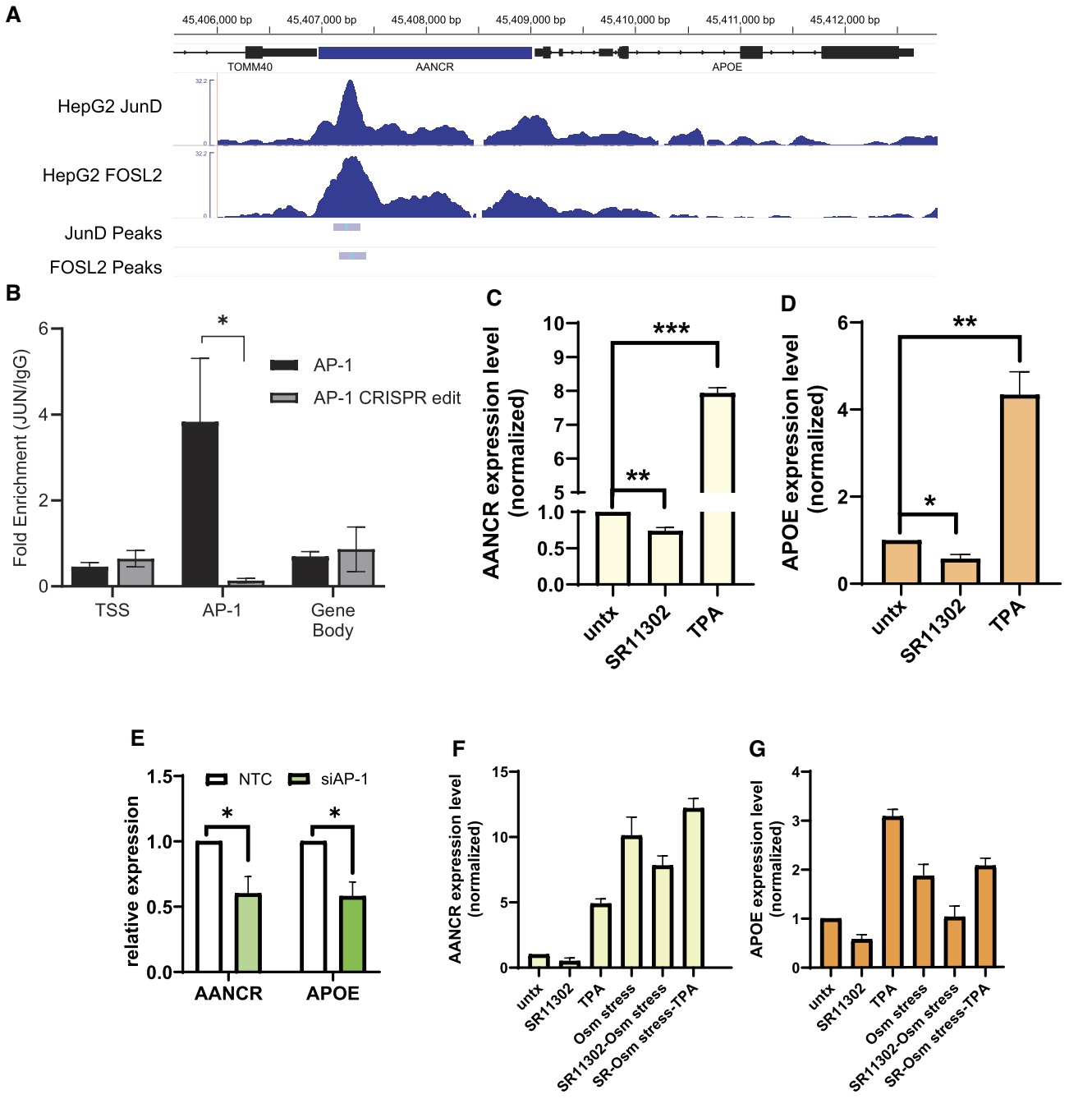

Figure 6. AP-1 regulates AANCR and subsequently *APOE* expression in astrocytes. Data from the ENCODE consortium showing JUN and FOSL2 that constitute AP-1 bind to AANCR (**A**). CRISPR-mediated mutation of the AP-1 site in AANCR results in a decrease in JUN occupancy as found by ChIP assay ($N = 2$, $P < 0.05$; *t*-test) (**B**). In astrocytes, SR11302 which inhibits AP-1 decreases AANCR (**C**) and *APOE* expression (**D**), whereas TPA, an activator of AP-1 increases AANCR (**C**) and *APOE* expression (**D**). siRNA against the AP-1 site of AANCR decreases AANCR and *APOE* expression (**E**). In astrocytes, osmotic stress increases AANCR (**F**) and *APOE* (**G**) expression, and this induction can be suppressed by SR11302 and rescued with TPA (F and G) (for C–G, $n \geq 3$, error bar = S.E.M. * $P < 0.05$, ** $P < 0.005$, *** $P < 0.001$).

AANCR. The results showed that AANCR expression in response to oxidative stress is dependent on the activation or phosphorylation of JUN. Figure 7G showed that in microglia where JUN cannot be activated, AANCR induction is significantly ($P < 0.001$, *t*-test) reduced in response to antimycin A treatment.

Together our results elucidated the upstream signaling pathway that activates AANCR in response to mitochondrial stress. In response to stress, ATM is activated which then phosphorylates ERK. The pERK then phosphorylates JUN to activate the AP-1 site that promotes the transcription of AANCR, and therefore the expression of *APOE*.

In astrocytes, reducing the expression of AANCR and/or APOE confers a less inflammatory expression phenotype

After finding that AANCR regulates *APOE* downstream of the ATM-ERK-AP1 pathway, we turned to examine the genes that are regulated by AANCR and *APOE*. We silenced

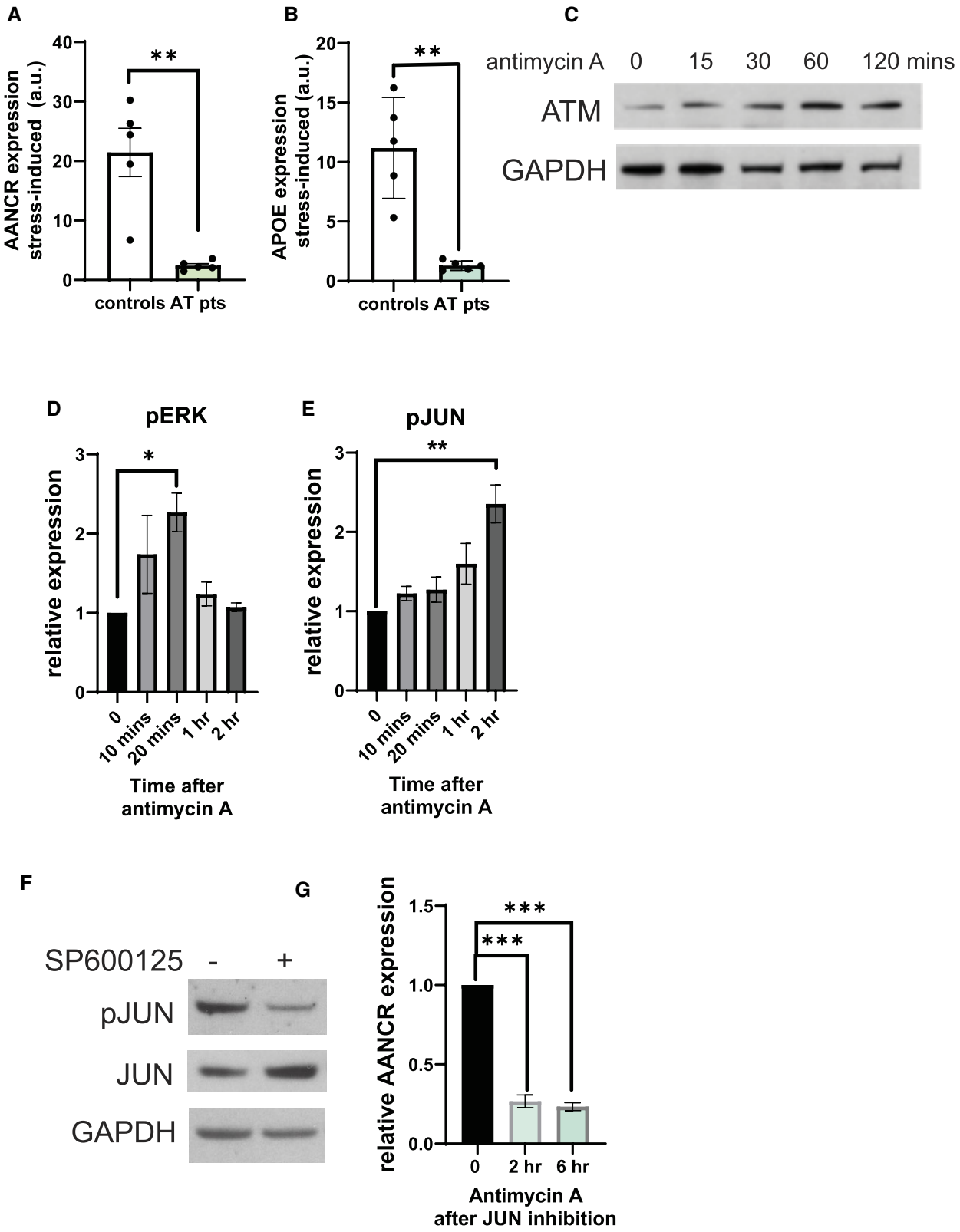

Figure 7. ATM–ERK–JUN regulates AANCR expression. In response to osmotic stress, B-cells from controls induce AANCR and *APOE* expression while those from AT-patients with ATM null mutations induce significantly less AANCR and *APOE* (**A** and **B**). Data from each individual are shown as a dot. In microglia, ATM is induced within 15 mins of antimycin A treatment; representative western blot ($n = 3$, data quantified) is shown in (**C**). Following ATM induction, ERK is phosphorylated (**D**) and subsequently JUN is phosphorylated (**E**) in microglia treated with antimycin A; pERK and pJUN were measured by immunoblots. The phosphorylation of JUN was inhibited by treatment with SP600125 (**F**) and in microglia where phosphorylation of JUN is inhibited, AANCR is induced at a significantly lower level (**G**) ($n \geq 3$, error bar = S.E.M. * $P < 0.05$, ** $P < 0.005$, *** $P < 0.001$).

AANCR and *APOE*, each with five different siRNAs or ASO. In total, there were 10 gene silencing experiments plus nontarget controls, NTC. After validating that each siRNA and the ASO decreased AANCR and *APOE* expression significantly (Supplementary Figure S6), we carried out cDNA-sequencing with at least 150 million reads per sample. Traditionally, these experiments have been referred to as RNA-sequencing, but since the RNA is reverse transcribed to cDNA which is then sequenced, we called them cDNA-sequencing (to contrast them to actual RNA-sequencing as in Oxford Nanopore direct RNA sequencing experiments). AANCR and *APOE* knockdown resulted in highly similar expression profiles. Figure 8A is a correlation matrix; the diagonal is lined with comparisons of the same samples, and the off-diagonal comparisons of the AANCR and *APOE* knockdown samples are highly similar to the self-comparisons. The similarity in expression profiles after AANCR and *APOE* knockdown provides further evidence that *APOE* is a major target gene of AANCR.

Next, using the cDNA-sequencing results, we looked for genes whose expression levels changed significantly following AANCR and *APOE* knockdown. Among the about 12 000 expressed genes, we found that *APOE* expression decreased by an average of 77% and 84%, respectively ($P < 2 \times 10^{-8}$, *t*-tests). Additionally, 597 other genes also changed expression significantly (Bonferroni corrected $P < 0.05$, *t*-test) and by at least 2-fold between controls and in the knockdown samples (Supplementary Table S1). Among these 598 genes are *C3* and other genes (e.g. *CFB, C4B*) (Table 1) in the complement pathway that characterizes A1 astrocytes. The expression levels of these genes are significantly reduced in the astrocytes following AANCR and *APOE* knockdown. In contrast, the expression levels of genes such as *EMP1* and *S100A10* that characterize A2 astrocytes are increased (Table 1). Thus, it appears that the knockdown of *APOE* leads to a dampening of the inflammatory features of astrocytes.

RELA, also known as p65, is a component of dimeric transcription factor NF-κβ that activates inflammatory cytokines, and sequence variants in RELA are associated with inflammatory diseases such as inflammatory bowel disease (59–62). The expression level of *RELA* is significantly reduced (Figure 8B) in the astrocytes following both AANCR and *APOE* knockdown. The promoters of *CXCL1* and *CXCL2* contain NF-κβ binding sites, and their expression levels are regulated by RELA (63). The lower *RELA* expression likely contributes to the reduction in the chemokines and the dampening of the inflammatory features in the astrocytes with reduced *APOE* expression.

Furthermore, network analysis of the 598 differentially expressed genes with *k*-means clustering (24) revealed a group of 115 genes that are significantly enriched (Supplementary Table S1, Benjamini–Hochberg corrected $P < 10^{-10}$ as per the STRING analysis (24)) for interaction with RIG1 (64–68), a key receptor in the antiviral innate immune response. RIG1 detects RNA viruses, such as the coronavirus, and triggers the interferon response (69–73). Polymorphism in *APOE* has been implicated in influencing individual susceptibility to RNA viruses (74–76). Figure 8C is a network of these genes based on the confidence model of network edges (24). The expression levels of these interferon-related genes such as *ARMC5, IRF7, ISG15, ISG20* and *DDX58* (RIG1) decreased significantly following AANCR and *APOE* knockdown (Table 2). These interferon-related genes are involved in neuroinflammation and found to be dysregulated in aging models and patients with early stages of Alzheimer's disease (77–81). These results further show reducing AANCR and therefore *APOE* expression may lessen neuroinflammation.

Almost 20% (110 genes, Supplementary Table S1, Benjamini–Hochberg corrected $P = 5 \times 10^{-6}$ as per the STRING analysis (24)) of the 598 genes, interact with ESRβ. Estrogen receptor β plays a key role in transcription regulation and neuroprotection against inflammation (82–84). ESRβ expression level in astrocytes decreased (by 31% siAANCR, 50% siAPOE, $n = 5$ each) following AANCR and *APOE* knockdown, although it did not reach our significance cutoff. Among the genes in the ESRβ interactome are transcription regulators such as *ARID5A*, *CACTIN*, *CC2D1A, CIC* and *SF3A2* that influence transcript stability, splicing, and gene expression as well as genes such as *DDX49*, *DHX37*, *MRPL4* and *RPLP1* (Table 3) that regulate translation. This interactome also includes two genes that are significantly down-regulated by >50%, they are *MIF*, the migration inhibitory factor ($P < 10^{-9}$, *t*-test) and *UNC93B1* ($P < 10^{-6}$, *t*-test), a Toll-like receptor regulator (Figure 8D). MIF is a cytokine that regulates immune response and is expressed by various cell types in the CNS and its overexpression has been implicated in inflammatory processes that worsen pathology in Alzheimer's Disease (85–89). Ibudilast, an anti-inflammatory drug that decreases MIF has been proposed as a treatment for Alzheimer's Disease (90–92). UNC93B1 regulates immune responses by stabilizing and controlling the trafficking of Toll-like receptors such as TLR7 and TLR9 from the endoplasmic reticulum to endolysosomes and contributes to neuroinflammation (93–96). Together, these findings support AANCR-*APOE*'s role in conferring inflammatory features of astrocytes.

AANCR knockdown and APOE knockdown decrease mitochondrial function in astrocytes

Among the 598 differentially expressed genes following the knockdown of AANCR and *APOE* in astrocytes, we found a significant proportion of mitochondrial genes (Supplementary Table S1, FDR $= 2 \times 10^{-4}$). This includes 32 mitochondrial-related genes such as *NDUFA3*, *NDUFB7* and *NDUFS7*, which are integral components of Complex I in the electron transport chain. These genes are also cataloged in Mitocarta 3.0, a comprehensive inventory of mammalian mitochondrial proteins and pathways (97). Figure 9A shows a heatmap of these mitochondrial genes, all of which exhibit decreased expression following the knockdown of AANCR and *APOE*.

To further investigate the impact of this gene expression alteration, we assessed mitochondrial respiration and glycolysis in astrocytes (83,84). Our results showed that after AANCR knockdown, there was a significant reduction in the oxygen consumption of astrocytes ($P < 0.0001$; Figure 9B), consistent with the observed changes in gene expression. Typically, astrocytes respond to inflammation by increasing oxygen consumption to enhance their metabolic functions. Given that the reduction in AANCR and *APOE* expression was associated with a less inflammatory gene expression phenotype, a corresponding decrease in metabolic activity was observed.

Additionally, we explored the effect of decreased AANCR-*APOE* expression on glycolysis. We noted a significant reduction (Figure 9C, >3-fold, $P = 5 \times 10^{-8}$, *t*-test) in the expression of phosphofructokinase, a key enzyme in

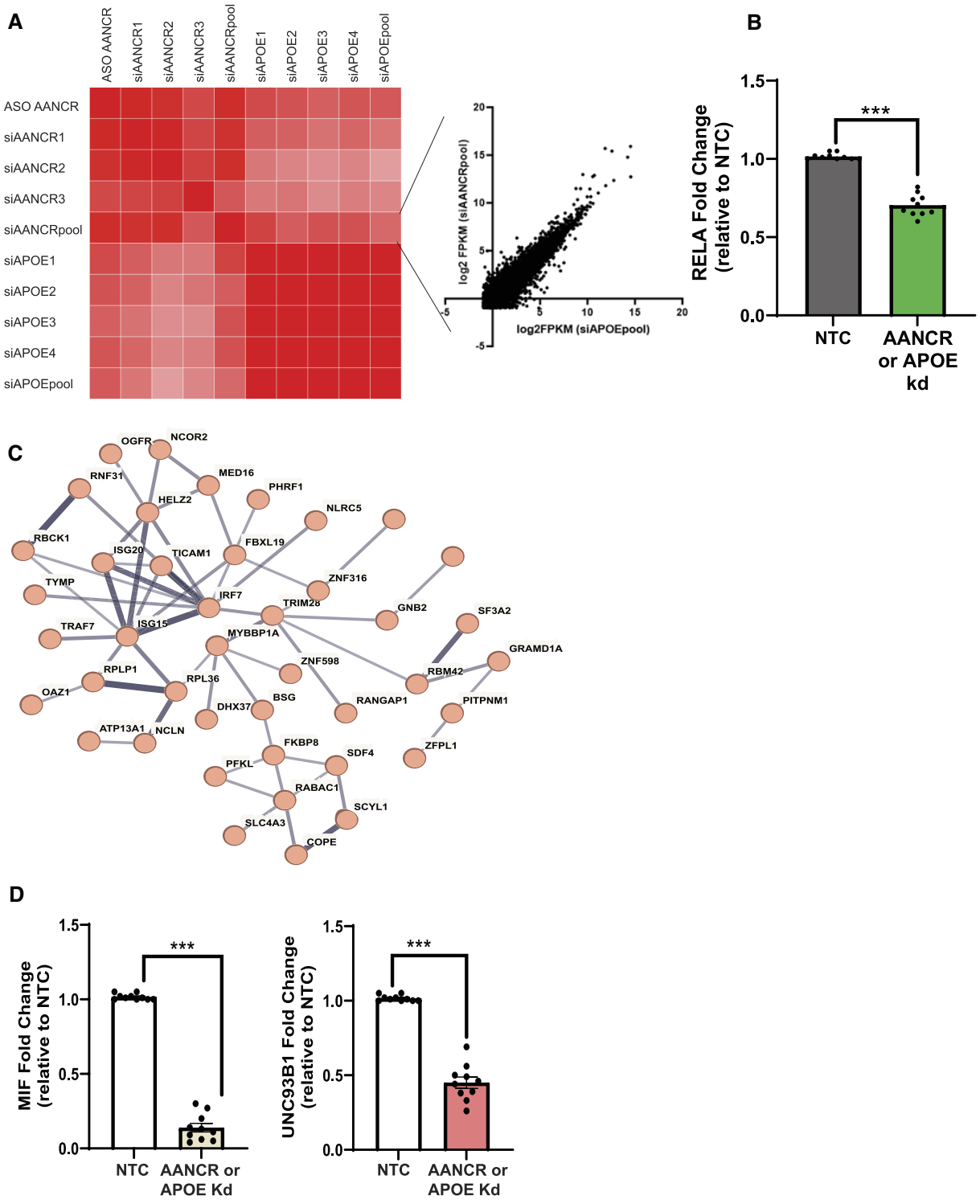

Figure 8. AANCR and APOE knockdown confer a less inflammatory expression phenotype. A correlation matrix with genes whose expression levels changed significantly in astrocytes with AANCR and *APOE* knockdown, a correlation plot for AANCR knockdown with pooled siRNA and *APOE* knockdown with pooled siRNAs; data based on cDNA-sequencing of the samples (**A**). The expression of *RELA* decreased significantly after AANCR or *APOE* knockdown (**B**). Genes that changed significantly following AANCR and *APOE* knockdown include those that encode proteins that interact with RIG-1, per data in Biogrid. A network of their interactions as determined by STRING using the confidence model for edges (**C**). Expression levels of Migration Inhibitory Factor, *MIF* and unc-93 homolog B1, *UNC93B1* were also reduced following AANCR and *APOE* knockdown (**D**) ($n = 5$ siAANCR experiments, $n = 5$ siAPOE experiments, error bar = S.E.M. $^{***}P < 0.0001$).

Table 1. Following AANCR and *APOE* knockdown, the expression levels of genes that are associated with A1- and A2-like astrocytes changed significantly

Gene name	Markers	Fold change AANCR kd vs. NTC	Fold change APOE kd vs. NTC	Nominal *P*-value (*t*-test combined AANCR and APOE kd)
C3	A1	0.14	0.57	7.64E-06
C4B	A1	0.24	0.54	8.53E-06
CFB	A1	0.28	0.33	7.37E-06
CHI3L2	A2	1.42	1.50	4.38E-08
S100A10	A2	1.23	1.35	4.88E-06
B3GNT5	A2	1.25	1.34	1.26E-06
TM4SF1	A2	1.36	1.30	4.51E-06
EMP1	A2	1.13	1.23	8.31E-06
FZD6	A2	1.22	1.21	1.50E-07

The changes following AANCR and *APOE* knockdown are shown to highlight the consistencies upon gene knockdown. Sample sizes are $n = 5$ for AANCR knockdown and $n = 5$ for *APOE* knockdown. The *P*-values are derived from Student's t-tests combining the 10 sets of knockdown data.

Table 2. Interferon-related genes whose expression levels were reduced significantly following AANCR and *APOE* knockdown

Gene name	Fold change AANCR kd vs. NTC	Fold Change APOE kd vs. NTC	Nominal *P*-value (*t*-test combined AANCR and APOE kd)
ARMC5	0.33	0.35	2.66E-09
IRF7	0.24	0.27	3.32E-09
ISG15	0.07	0.07	7.59E-14
ISG20	0.27	0.26	7.61E-09
DDX58	0.30	0.44	3.13E-09

The changes following AANCR and *APOE* knockdown are shown to highlight the consistencies upon gene knockdown. Sample sizes are $n = 5$ for AANCR knockdown and $n = 5$ for *APOE* knockdown. The *P*-values are derived from Student's *t*-tests combining the 10 sets of knockdown data.

glycolysis (98–101). To determine if this decrease in gene expression translated to functional changes, we measured the extracellular acidification rate (ECAR), a marker of glycolytic activity. Consistent with our hypothesis, there was a significant decrease in glycolysis following the reduction in AANCR expression ($P < 0.0001$, ANOVA; Figure 9D). The reduction in their oxygen consumption and glycolytic activity following AANCR-*APOE* knockdown is consistent with a decrease in inflammatory features of the astrocytes (102–104).

Together, the gene expression profiles, and metabolic activities suggest that AANCR and *APOE* confer on astrocytes an inflammatory phenotype.

Discussion

In this study, we focused on the enhancer RNA, AANCR, and found that its transcripts are needed to promote *APOE* expression. We elucidated the regulation of AANCR by the ATM-ERK-AP1 pathway and showed that it functions by conferring an inflammatory phenotype to astrocytes.

High-throughput screening has identified hundreds of thousands to millions of enhancers and many of them are transcribed leading to enhancer RNAs (1). To dissect these regulatory elements, methods such as massively parallel reporter assays (105) and CRISPR screens have probed the activities of enhancers (106,107). Additionally, genetic studies identified that sequence variants in enhancers are enriched for susceptibility alleles for complex diseases (108,109) leading to the term enhanceropathies (110). However, connecting the alteration of enhancers to human diseases remains challenging (111). To figure out how enhancer variants confer disease susceptibility and to leverage enhancer function for therapeutic intervention require transitioning from high-throughput analyses to focusing on the details of individual enhancers.

Table 3. Genes that encode proteins that interact with ESRβ according to data from Biogrid

Gene name	Fold change AANCR kd vs. NTC	Fold change APOE kd vs. NTC	Nominal *P*-value (*t*-test combined AANCR and APOE kd)
ARID5A	0.40	0.32	4.42E-08
CACTIN	0.50	0.42	3.54E-08
CC2D1A	0.48	0.27	2.30E-07
CIC	0.41	0.34	2.90E-09
SF3A2	0.39	0.24	4.41E-08
DDX49	0.38	0.29	1.11E-08
DHX37	0.42	0.40	3.67E-09
MRPL4	0.39	0.22	1.01E-08
RPLP1	0.47	0.32	2.26E-07

The changes following AANCR and *APOE* knockdown are shown to highlight the consistencies upon gene knockdown. Sample sizes are $n = 5$ for AANCR knockdown and $n = 5$ for *APOE* knockdown. The *P*-values are derived from Student's *t*-tests combining the 10 sets of knockdown data.

Previously, we identified AANCR as an enhancer RNA of *APOE* in peripheral cells and a genetic modifier of Alzheimer's Disease (16). Here, we focused on the function and regulation of AANCR in cells relevant to neurodegenerative diseases. We felt that distinguishing whether AANCR transcription alone or the transcript itself is needed to regulate *APOE* expression is important. Understanding this distinction can guide strategies for altering *APOE* expression as a therapeutic option for Alzheimer's Disease and other conditions such as neuroinflammation where *APOE* has been implicated. We found that AANCR transcription is not sufficient but rather AANCR transcripts are needed to regulate *APOE* expression. This shows that siRNAs and ASOs against AANCR are therapeutic options for altering *APOE* expression. Determining that the ATM-EKR-AP1 pathway regulates AANCR, and AANCR's role in promoting an inflammatory phenotype, improves our understanding of this enhancer RNA.

The discovery of key genetic modifiers such as *SMN2* in spinal muscular atrophy and *BCL11A* in sickle cell anemia and thalassemia, has paved the way for groundbreaking therapeutic interventions. For instance, Nusinersen, an RNA-based treatment for spinal muscular atrophy, enhances the inclusion of exon 7 in *SMN2*, leading to increased SMN protein production in patients (112). This advance has been instrumental in preventing fatalities and allowing patients to achieve developmental milestones (113,114). Similarly, Exagamglogene autotemcel, a CRISPR-based therapy for sickle-cell anemia and β-thalassemia targets *BCL11A* to reactivate fetal hemoglobin production (115). Results have shown a reduction or cessation of pain crises in sickle cell patients and an elimination of the need for transfusions in β-thalassemia patients. In this context, our research demonstrates that AANCR, a modifier of Alzheimer's Disease, regulates *APOE* expression in the nervous system. We found that targeting AANCR transcripts with RNA interference or RNaseH-mediated

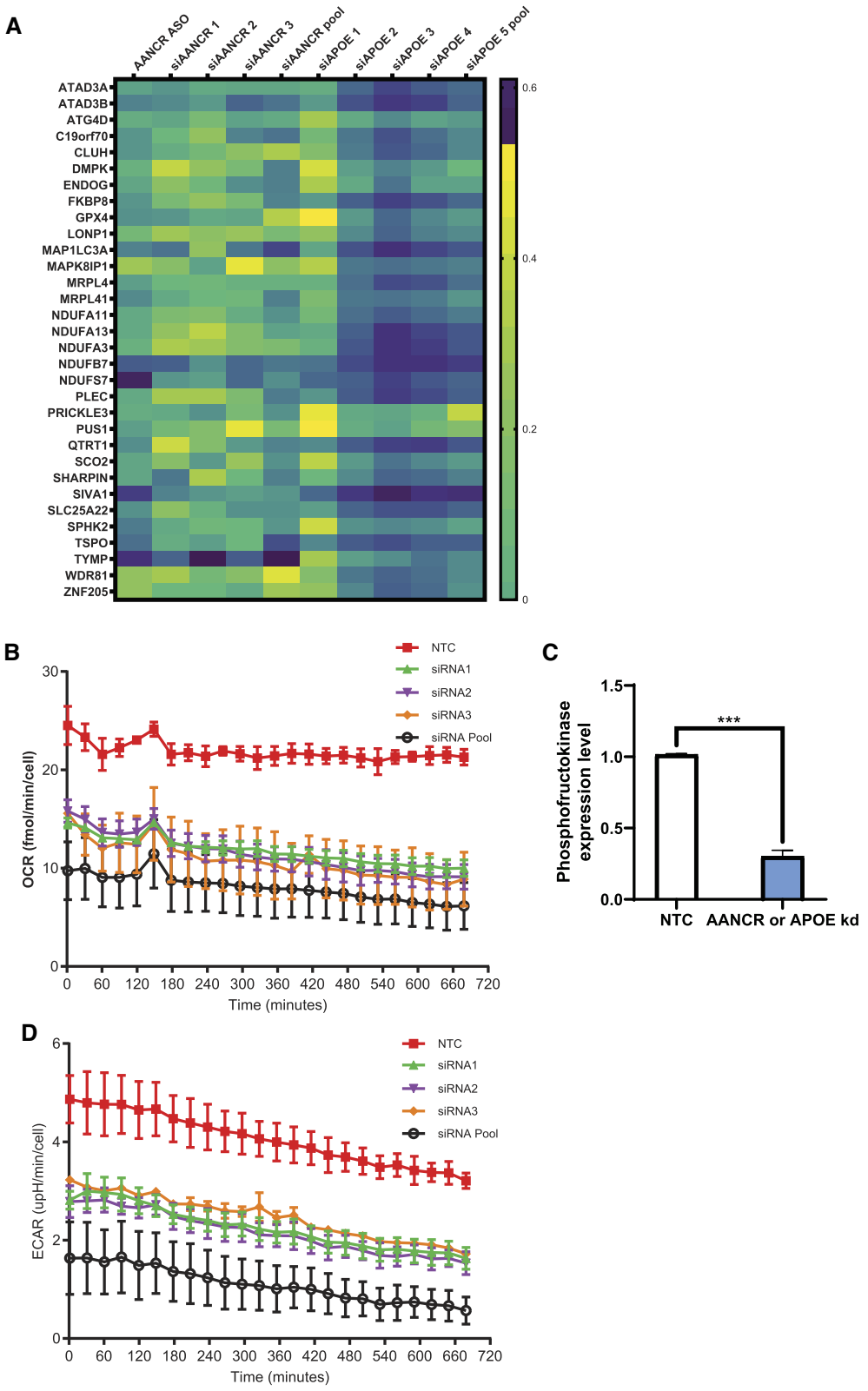

Figure 9. AANCR and APOE knockdown leads to a reduction in mitochondrial function Heat map showing expression of 32 mitochondrial-related genes downregulated by knockdown of AANCR and *APOE* (**A**). Seahorse assay of astrocytes after AANCR knockdown. The oxygen consumption rate (OCR) is significantly lower ($n = 3$, error bars = S.D., $P < 0.0001$; one-sided ANOVA (**B**). Expression levels of phosphofructokinase were significantly reduced following AANCR and APOE knockdown (**C**) ($n = 5$ siAANCR experiments, n = 5 siAPOE experiments, error bar = S.E.M. $***P < 0.0001$, one-sided ANOVA). Seahorse assay of astrocytes after AANCR knockdown shows that the extracellular acidification rates (**D**) are significantly lower ($n = 3$ per treatment, error bars = S.D., $***P < 0.0001$, one-sided ANOVA).

degradation leads to lower *APOE* levels, which then reduces the inflammatory characteristics of astrocytes.

Previous research by Ben Barres and colleagues identified A1 astrocytes by their expression of *C3* and other complement genes and showed the neurotoxicity of these cells. In contrast, A2 astrocytes, characterized by their expression of S100A10, are more neuroprotective (116,117). Based on their findings, we suggest that by lowering *APOE* expression, one can shift astrocytes from an A1 to an A2 phenotype, a transition that could be advantageous in scenarios like acute CNS injury or infections where reducing inflammation is desired. Future investigations will focus on the potential of targeting AANCR in scenarios where mitigating neuroinflammation could be beneficial.

The mechanism by which enhancer RNAs regulate their target genes is mostly unknown. The bromodomain and extra-terminal domain (BET) and Jumonji families of proteins are involved in transcriptional control of enhancers (118–121). Identifying the mechanism by which AANCR regulates *APOE* will be an important step. Our previous work in PROseq analysis did not identify paused RNA polymerase II in the promoter of *APOE* so AANCR is not likely to interact with NELF (122,123) or other protein complexes that pause proximal promoter transcription. Our early results suggest that BRD4 and JMJD6 interact with AANCR and *APOE* but much analysis is needed to understand the mechanism by which AANCR regulates *APOE*.

In summary, our study identified the RNA transcripts of an enhancer as a key regulator of *APOE* expression in various cell types in the nervous system at baseline and in stress responses. We also uncovered the ATM-ERK-AP1 pathway that regulates AANCR and demonstrated an association of AANCR-*APOE* with the inflammatory phenotype of astrocytes. Future investigation into altering AANCR and/or *APOE* expression is warranted to examine the potential to modulate inflammation. We posit that the dissection of the nucleic acid biology of enhancers will lead to a better understanding and therapeutic options for enhanceropathies.

Data availability

Sequencing data were deposited to NCBI GEO https://www.ncbi.nlm.nih.gov/geo/query/acc.cgi?acc=GSE263862.

Supplementary data

Supplementary Data are available at NAR Online.

Acknowledgements

We thank Drs Joshua Burdick and Don Delker for bioinformatic analyses. Drs Alan Bruzel, Nancy Cox and Robert Crouch for discussions.

Funding

Warren Alpert Foundation (to V.G.C.); NIH [ES034919 to V.G.C., 1RF1AG059751 to R.W.M.]; ASN-Kidney Cure career development award (to J.A.W.) Intramural Research Program of the National Institutes of Health, National Institute of Environmental Health Sciences [ES103361 to J.A.W., ES103331 to J.R.]; National Institute of Neurological Disorders and Stroke NS009455 (to C.G.). Funding for open access charge: NIH grants.

Conflict of interest statement

None declared.

References

1. Gasperini,M., Hill,A.J., McFaline-Figueroa,J.L., Martin,B., Kim,S., Zhang,M.D., Jackson,D., Leith,A., Schreiber,J., Noble,W.S., *et al.* (2019) A genome-wide framework for mapping gene regulation via cellular genetic screens. *Cell*, **176**, 377–390.
2. Martinez-Ara,M., Comoglio,F., van Arensbergen,J. and van Steensel,B. (2022) Systematic analysis of intrinsic enhancer-promoter compatibility in the mouse genome. *Mol. Cell*, **82**, 2519–2531.
3. Bergman,D.T., Jones,T.R., Liu,V., Ray,J., Jagoda,E., Siraj,L., Kang,H.Y., Nasser,J., Kane,M., Rios,A., *et al.* (2022) Compatibility rules of human enhancer and promoter sequences. *Nature*, **607**, 176–184.
4. Andersson,R., Gebhard,C., Miguel-Escalada,I., Hoof,I., Bornholdt,J., Boyd,M., Chen,Y., Zhao,X., Schmidl,C., Suzuki,T., *et al.* (2014) An atlas of active enhancers across human cell types and tissues. *Nature*, **507**, 455–461.
5. Hnisz,D., Abraham,B.J., Lee,T.I., Lau,A., Saint-André,V., Sigova,A.A., Hoke,H.A. and Young,R.A. (2013) Super-enhancers in the control of cell identity and disease. *Cell*, **155**, 934–947.
6. De Santa,F., Barozzi,I., Mietton,F., Ghisletti,S., Polletti,S., Tusi,B.K., Muller,H., Ragoussis,J., Wei,C.-L. and Natoli,G. (2010) A large fraction of extragenic RNA pol II transcription sites overlap enhancers. *PLoS Biol.*, **8**, e1000384.
7. Kim,T.-K., Hemberg,M., Gray,J.M., Costa,A.M., Bear,D.M., Wu,J., Harmin,D.A., Laptewicz,M., Barbara-Haley,K., Kuersten,S., *et al.* (2010) Widespread transcription at neuronal activity-regulated enhancers. *Nature*, **465**, 182–187.
8. Ørom,U.A., Derrien,T., Beringer,M., Gumireddy,K., Gardini,A., Bussotti,G., Lai,F., Zytnicki,M., Notredame,C., Huang,Q., *et al.* (2010) Long noncoding RNAs with enhancer-like function in human cells. *Cell*, **143**, 46–58.
9. Tuan,D., Kong,S. and Hu,K. (1992) Transcription of the hypersensitive site HS2 enhancer in erythroid cells. *Proc. Natl. Acad. Sci. U.S.A.*, **89**, 11219–11223.
10. Kim,T.-K., Hemberg,M. and Gray,J.M. (2015) Enhancer RNAs: a class of long noncoding RNAs synthesized at enhancers. *Cold Spring Harb. Perspect. Biol.*, **7**, a018622.
11. Statello,L., Guo,C.-J., Chen,L.-L. and Huarte,M. (2021) Gene regulation by long non-coding RNAs and its biological functions. *Nat. Rev. Mol. Cell Biol.*, **22**, 96–118.
12. Xiang,J.-F., Yin,Q.-F., Chen,T., Zhang,Y., Zhang,X.-O., Wu,Z., Zhang,S., Wang,H.-B., Ge,J., Lu,X., *et al.* (2014) Human colorectal cancer-specific CCAT1-L lncRNA regulates long-range chromatin interactions at the MYC locus. *Cell Res.*, **24**, 513–531.
13. Gupta,R.A., Shah,N., Wang,K.C., Kim,J., Horlings,H.M., Wong,D.J., Tsai,M.-C., Hung,T., Argani,P., Rinn,J.L., *et al.* (2010) Long non-coding RNA HOTAIR reprograms chromatin state to promote cancer metastasis. *Nature*, **464**, 1071–1076.
14. Bhan,A. and Mandal,S.S. (2015) LncRNA HOTAIR: a master regulator of chromatin dynamics and cancer. *Biochim. Biophys. Acta. (BBA)*, **1856**, 151–164.
15. Lettice,L.A., Heaney,S.J.H., Purdie,L.A., Li,L., de Beer,P., Oostra,B.A., Goode,D., Elgar,G., Hill,R.E. and de Graaff,E. (2003) A long-range Shh enhancer regulates expression in the developing limb and fin and is associated with preaxial polydactyly. *Hum. Mol. Genet.*, **12**, 1725–1735.
16. Watts,J.A., Grunseich,C., Rodriguez,Y., Liu,Y., Li,D., Burdick,J.T., Bruzel,A., Crouch,R.J., Mahley,R.W., Wilson,S.H., *et al.* (2022)

A common transcriptional mechanism involving R-loop and RNA abasic site regulates an enhancer RNA of APOE. *Nucleic Acids Res*., **50**, 12497–12514.
17. Kwak,H., Fuda,N.J., Core,L.J. and Lis,J.T. (2013) Precise maps of RNA polymerase reveal how promoters direct initiation and pausing. *Science*, **339**, 950–953.
18. Wu,T.D. and Nacu,S. (2010) Fast and SNP-tolerant detection of complex variants and splicing in short reads. *Bioinformatics*, **26**, 873–881.
19. Trapnell,C., Roberts,A., Goff,L., Pertea,G., Kim,D., Kelley,D.R., Pimentel,H., Salzberg,S.L., Rinn,J.L. and Pachter,L. (2012) Differential gene and transcript expression analysis of RNA-seq experiments with TopHat and Cufflinks. *Nat. Protoc*., **7**, 562–578.
20. Love,M.I., Huber,W. and Anders,S. (2014) Moderated estimation of fold change and dispersion for RNA-seq data with DESeq2. *Genome Biol*., **15**, 550.
21. Watts,J.A., Zhang,C., Klein-Szanto,A.J., Kormish,J.D., Fu,J., Zhang,M.Q. and Zaret,K.S. (2011) Study of FoxA pioneer factor at silent genes reveals rfx-repressed enhancer at Cdx2 and a potential indicator of esophageal adenocarcinoma development. *PLoS Genet*., **7**, e1002277.
22. Fernandopulle,M.S., Prestil,R., Grunseich,C., Wang,C., Gan,L. and Ward,M.E. (2018) Transcription factor-mediated differentiation of Human iPSCs into neurons. *Curr. Protoc. Cell Biol*., **79**, e51.
23. Ran,F.A., Hsu,P.D., Wright,J., Agarwala,V., Scott,D.A. and Zhang,F. (2013) Genome engineering using the CRISPR-Cas9 system. *Nat. Protoc*., **8**, 2281–2308.
24. Szklarczyk,D., Kirsch,R., Koutrouli,M., Nastou,K., Mehryary,F., Hachilif,R., Gable,A.L., Fang,T., Doncheva,N.T., Pyysalo,S., *et al.* (2023) The STRING database in 2023: protein-protein association networks and functional enrichment analyses for any sequenced genome of interest. *Nucleic Acids Res*., **51**, D638–D646.
25. Sherman,B.T., Hao,M., Qiu,J., Jiao,X., Baseler,M.W., Lane,H.C., Imamichi,T. and Chang,W. (2022) DAVID: a web server for functional enrichment analysis and functional annotation of gene lists (2021 update). *Nucleic Acids Res*., **50**, W216–W221.
26. Rodriguez,J., Ren,G., Day,C.R., Zhao,K., Chow,C.C. and Larson,D.R. (2019) Intrinsic dynamics of a Human gene reveal the basis of expression heterogeneity. *Cell*, **176**, 213–226.
27. Hoffman,J.A., Trotter,K.W., Day,C.R., Ward,J.M., Inoue,K., Rodriguez,J. and Archer,T.K. (2022) Multimodal regulatory elements within a hormone-specific super enhancer control a heterogeneous transcriptional response. *Mol. Cell*, **82**, 803–815.
28. Blumenfeld,J., Yip,O., Kim,M.J. and Huang,Y. (2024) Cell type-specific roles of APOE4 in Alzheimer disease. *Nat. Rev. Neurosci*., **25**, 91–110.
29. González-Reyes,R.E., Nava-Mesa,M.O., Vargas-Sánchez,K., Ariza-Salamanca,D. and Mora-Muñoz,L. (2017) Involvement of astrocytes in Alzheimer's disease from a neuroinflammatory and oxidative stress perspective. *Front.Mol. Neurosci*., **10**, 427.
30. Onyango,I.G. and Khan,S.M. (2006) Oxidative stress, mitochondrial dysfunction, and stress signaling in Alzheimer's disease. *Curr. Alzheimer Res*., **3**, 339–349.
31. Rieske,J.S., Baum,H., Stoner,C.D. and Lipton,S.H. (1967) On the antimycin-sensitive cleavage of complex III of the mitochondrial Respiratory chain. *J. Biol. Chem*., **242**, 4854–4866.
32. Rieske,J.S. and Zaugg,W.S. (1962) The inhibition by antimycin A of the cleavage of one of the complexes of the respiratory chain. *Biochem. Biophys. Res. Commun*., **8**, 421–426.
33. Wynne,M.E., Ogunbona,O., Lane,A.R., Gokhale,A., Zlatic,S.A., Xu,C., Wen,Z., Duong,D.M., Rayaprolu,S., Ivanova,A., *et al.* (2023) APOE expression and secretion are modulated by mitochondrial dysfunction. *eLife*, **12**, e85779.
34. Butterfield,D.A. (1997) beta-amyloid-associated free radical oxidative stress and neurotoxicity: implications for Alzheimer's disease. *Chem. Res. Toxicol*., **10**, 495–506.
35. Allan Butterfield,D., Castegna,A., Lauderback,C.M. and Drake,J. (2002) Evidence that amyloid beta-peptide-induced lipid peroxidation and its sequelae in Alzheimer's disease brain contribute to neuronal death. *Neurobiol. Aging*, **23**, 655–664.
36. Gu,L. and Guo,Z. (2013) Alzheimer's Aβ42 and Aβ40 peptides form interlaced amyloid fibrils. *J. Neurochem*., **126**, 305–311.
37. Cheignon,C., Tomas,M., Bonnefont-Rousselot,D., Faller,P., Hureau,C. and Collin,F. (2018) Oxidative stress and the amyloid beta peptide in Alzheimer's disease. *Redox. Biol*., **14**, 450–464.
38. Behl,C. (1997) Amyloid β-protein toxicity and oxidative stress in Alzheimer's disease. *Cell Tissue Res*., **290**, 471–480.
39. Miranda,S., Opazo,C., Larrondo,L.F., Muñoz,F.J., Ruiz,F., Leighton,F. and Inestrosa,N.C. (2000) The role of oxidative stress in the toxicity induced by amyloid β-peptide in Alzheimer's disease. *Prog. Neurobiol*., **62**, 633–648.
40. Nikitidou,E., Khoonsari,P.E., Shevchenko,G., Ingelsson,M., Kultima,K. and Erlandsson,A. (2017) Increased release of apolipoprotein E in extracellular vesicles following amyloid-β protofibril exposure of neuroglial co-cultures. *J. Alzheimers Dis*., **60**, 305–321.
41. Rauscher,F.J., Voulalas,P.J., Franza,B.R. and Curran,T. (1988) Fos and Jun bind cooperatively to the AP-1 site: reconstitution in vitro. *Genes Dev*., **2**, 1687–1699.
42. Karin,M., Liu,Z.g. and Zandi,E. (1997) AP-1 function and regulation. *Curr. Opin. Cell Biol*., **9**, 240–246.
43. Vesely,P.W., Staber,P.B., Hoefler,G. and Kenner,L. (2009) Translational regulation mechanisms of AP-1 proteins. *Mutat. Res./Rev. Mutat. Res*., **682**, 7–12.
44. Shaulian,E. and Karin,M. (2001) AP-1 in cell proliferation and survival. *Oncogene*, **20**, 2390–2400.
45. Huang,C., Ma,W.-Y., Dawson,M.I., Rincon,M., Flavell,R.A. and Dong,Z. (1997) Blocking activator protein-1 activity, but not activating retinoic acid response element, is required for the antitumor promotion effect of retinoic acid. *Proc. Natl. Acad. Sci. U.S.A*., **94**, 5826–5830.
46. Lee,W., Mitchell,P. and Tjian,R. (1987) Purified transcription factor AP-1 interacts with TPA-inducible enhancer elements. *Cell*, **49**, 741–752.
47. Irarrazabal,C.E., Liu,J.C., Burg,M.B. and Ferraris,J.D. (2004) ATM, a DNA damage-inducible kinase, contributes to activation by high NaCl of the transcription factor TonEBP/OREBP. *Proc. Natl. Acad. Sci. U.S.A*., **101**, 8809–8814.
48. Guo,Z., Kozlov,S., Lavin,M.F., Person,M.D. and Paull,T.T. (2010) ATM activation by oxidative stress. *Science*, **330**, 517–521.
49. Tai,P. and Ascoli,M. (2011) Reactive oxygen species (ROS) play a critical role in the cAMP-induced activation of Ras and the phosphorylation of ERK1/2 in Leydig cells. *Mol. Endocrinol*., **25**, 885–893.
50. Wu,H., Li,H., Wu,X., Zhao,J. and Guo,J. (2008) Reactive oxygen species mediate ERK activation through different Raf-1-dependent signaling pathways following cerebral ischemia. *Neurosci. Lett*., **432**, 83–87.
51. Keshari,R.S., Verma,A., Barthwal,M.K. and Dikshit,M. (2013) Reactive oxygen species-induced activation of ERK and p38 MAPK mediates PMA-induced NETs release from human neutrophils. *J. Cell. Biochem*., **114**, 532–540.
52. Gurjar,M.V., Deleon,J., Sharma,R.V. and Bhalla,R.C. (2001) Role of reactive oxygen species in IL-1β-stimulated sustained ERK activation and MMP-9 induction. *Am. J. Physiol. Heart Circul. Physiol*., **281**, H2568–H2574.
53. El-Najjar,N., Chatila,M., Moukadem,H., Vuorela,H., Ocker,M., Gandesiri,M., Schneider-Stock,R. and Gali-Muhtasib,H. (2010) Reactive oxygen species mediate thymoquinone-induced apoptosis and activate ERK and JNK signaling. *Apoptosis*, **15**, 183–195.
54. Monick,M.M., Powers,L.S., Barrett,C.W., Hinde,S., Ashare,A., Groskreutz,D.J., Nyunoya,T., Coleman,M., Spitz,D.R. and Hunninghake,G.W. (2008) Constitutive ERK MAPK activity regulates macrophage ATP production and mitochondrial Integrity1. *J. Immunol*., **180**, 7485–7496.

55. Garg,T.K. and Chang,J.Y. (2003) Oxidative stress causes ERK phosphorylation and cell death in cultured retinal pigment epithelium: prevention of cell death by AG126 and 15-deoxy-delta 12, 14-PGJ2. *BMC Ophthalmol.*, **3**, 5.
56. Khalil,A., Morgan,R.N., Adams,B.R., Golding,S.E., Dever,S.M., Rosenberg,E., Povirk,L.F. and Valerie,K. (2011) ATM-dependent ERK signaling via AKT in response to DNA double-strand breaks. *Cell Cycle*, **10**, 481–491.
57. Tang,D., Wu,D., Hirao,A., Lahti,J.M., Liu,L., Mazza,B., Kidd,V.J., Mak,T.W. and Ingram,A.J. (2002) ERK activation mediates cell cycle arrest and apoptosis after DNA damage independently of p53. *J. Biol. Chem.*, **277**, 12710–12717.
58. Bennett,B.L., Sasaki,D.T., Murray,B.W., O'Leary,E.C., Sakata,S.T., Xu,W., Leisten,J.C., Motiwala,A., Pierce,S., Satoh,Y., *et al.* (2001) SP600125, an anthrapyrazolone inhibitor of Jun N-terminal kinase. *Proc. Natl. Acad. Sci. U.S.A.*, **98**, 13681–13686.
59. Xia,Y., Pauza,M.E., Feng,L. and Lo,D. (1997) RelB regulation of chemokine expression modulates local inflammation. *Am. J. Pathol.*, **151**, 375–387.
60. Beg,A.A. and Baldwin,A.S. (1993) The I kappa B proteins: multifunctional regulators of rel/NF-kappa B transcription factors. *Genes Dev.*, **7**, 2064–2070.
61. Gilmore,T.D. (1999) The rel/NF-κb signal transduction pathway: introduction. *Oncogene*, **18**, 6842–6844.
62. Liu,J.Z., van Sommeren,S., Huang,H., Ng,S.C., Alberts,R., Takahashi,A., Ripke,S., Lee,J.C., Jostins,L., Shah,T., *et al.* (2015) Association analyses identify 38 susceptibility loci for inflammatory bowel disease and highlight shared genetic risk across populations. *Nat. Genet.*, **47**, 979–986.
63. Burke,S.J., Lu,D., Sparer,T.E., Masi,T., Goff,M.R., Karlstad,M.D. and Collier,J.J. (2014) NF-κb and STAT1 control CXCL1 and CXCL2 gene transcription. *Am. J. Physiol. Endocrinol. Metab.*, **306**, E131.
64. Oughtred,R., Rust,J., Chang,C., Breitkreutz,B.-J., Stark,C., Willems,A., Boucher,L., Leung,G., Kolas,N., Zhang,F., *et al.* (2021) The BioGRID database: a comprehensive biomedical resource of curated protein, genetic, and chemical interactions. *Protein Sci.*, **30**, 187–200.
65. Wu,S.-F., Xia,L., Shi,X.-D., Dai,Y.-J., Zhang,W.-N., Zhao,J.-M., Zhang,W., Weng,X.-Q., Lu,J., Le,H.-Y., *et al.* (2020) RIG-I regulates myeloid differentiation by promoting TRIM25-mediated ISGylation. *Proc. Natl. Acad. Sci. U.S.A.*, **117**, 14395–14404.
66. Inn,K.-S., Gack,M.U., Tokunaga,F., Shi,M., Wong,L.-Y., Iwai,K. and Jung,J.U. (2011) Linear ubiquitin assembly complex negatively regulates RIG-I- and TRIM25-mediated type I interferon induction. *Mol. Cell*, **41**, 354–365.
67. Zhao,C., Denison,C., Huibregtse,J.M., Gygi,S. and Krug,R.M. (2005) Human ISG15 conjugation targets both IFN-induced and constitutively expressed proteins functioning in diverse cellular pathways. *Proc. Natl. Acad. Sci. U.S.A.*, **102**, 10200–10205.
68. Du,Y., Duan,T., Feng,Y., Liu,Q., Lin,M., Cui,J. and Wang,R.-F. (2018) LRRC25 inhibits type I IFN signaling by targeting ISG15-associated RIG-I for autophagic degradation. *EMBO J.*, **37**, 351–366.
69. Kawai,T. and Akira,S. (2008) Toll-like receptor and RIG-1-like receptor signaling. *Ann. N.Y. Acad. Sci.*, **1143**, 1–20.
70. Jiang,R., Ye,J., Zhu,B., Song,Y., Chen,H. and Cao,S. (2014) Roles of TLR3 and RIG-I in mediating the inflammatory response in mouse microglia following Japanese Encephalitis Virus infection. *J. Immunol. Res.*, **2014**, e787023.
71. Li,J., Liu,Y. and Zhang,X. (2010) Murine coronavirus induces type I interferon in oligodendrocytes through recognition by RIG-I and MDA5. *J. Virol.*, **84**, 6472–6482.
72. Takeuchi,O. and Akira,S. (2008) MDA5/RIG-I and virus recognition. *Curr. Opin. Immunol.*, **20**, 17–22.
73. Hu,Y., Li,W., Gao,T., Cui,Y., Jin,Y., Li,P., Ma,Q., Liu,X. and Cao,C. (2017) The severe acute Respiratory Syndrome coronavirus nucleocapsid inhibits type I interferon production by interfering with TRIM25-mediated RIG-I ubiquitination. *J. Virol.*, **91**, e02143-16.
74. Wang,C., Zhang,M., Garcia,G., Tian,E., Cui,Q., Chen,X., Sun,G., Wang,J., Arumugaswami,V. and Shi,Y. (2021) ApoE-isoform-dependent SARS-CoV-2 neurotropism and cellular response. *Cell Stem Cell*, **28**, 331–342.
75. Sheridan,D.A., Bridge,S.H., Felmlee,D.J., Crossey,M.M.E., Thomas,H.C., Taylor-Robinson,S.D., Toms,G.L., Neely,R.D.G. and Bassendine,M.F. (2012) Apolipoprotein-E and hepatitis C lipoviral particles in genotype 1 infection: evidence for an association with interferon sensitivity. *J. Hepatol.*, **57**, 32–38.
76. Wong,M.-T. and Chen,S.S.-L. (2016) Emerging roles of interferon-stimulated genes in the innate immune response to hepatitis C virus infection. *Cell Mol. Immunol*, **13**, 11–35.
77. Roy,E.R., Wang,B., Wan,Y., Chiu,G., Cole,A., Yin,Z., Propson,N.E., Xu,Y., Jankowsky,J.L., Liu,Z., *et al.* (2020) Type I interferon response drives neuroinflammation and synapse loss in Alzheimer disease. *J. Clin. Invest.*, **130**, 1912–1930.
78. Taylor,J.M., Minter,M.R., Newman,A.G., Zhang,M., Adlard,P.A. and Crack,P.J. (2014) Type-1 interferon signaling mediates neuro-inflammatory events in models of Alzheimer's disease. *Neurobiol. Aging*, **35**, 1012–1023.
79. Woodling,N.S., Wang,Q., Priyam,P.G., Larkin,P., Shi,J., Johansson,J.U., Zagol-Ikapitte,I., Boutaud,O. and Andreasson,K.I. (2014) Suppression of Alzheimer-associated inflammation by microglial prostaglandin-E2 EP4 receptor signaling. *J. Neurosci.*, **34**, 5882–5894.
80. Friedman,B.A., Srinivasan,K., Ayalon,G., Meilandt,W.J., Lin,H., Huntley,M.A., Cao,Y., Lee,S.-H., Haddick,P.C.G., Ngu,H., *et al.* (2018) Diverse brain myeloid expression profiles reveal distinct microglial activation states and aspects of Alzheimer's disease not evident in mouse models. *Cell Rep.*, **22**, 832–847.
81. de Rivero Vaccari,J.P., Brand,F.J., Sedaghat,C., Mash,D.C., Dietrich,W.D. and Keane,R.W. (2014) RIG-1 receptor expression in the pathology of Alzheimer's disease. *J. Neuroinflamm.*, **11**, 67.
82. Villa,A., Vegeto,E., Poletti,A. and Maggi,A. (2016) Estrogens, neuroinflammation, and neurodegeneration. *Endocr. Rev.*, **37**, 372–402.
83. Chakrabarti,M., Haque,A., Banik,N.L., Nagarkatti,P., Nagarkatti,M. and Ray,S.K. (2014) Estrogen receptor agonists for attenuation of neuroinflammation and neurodegeneration. *Brain Res. Bull.*, **109**, 22–31.
84. Dhandapani,K.M. and Brann,D.W. (2002) Estrogen-astrocyte interactions: implications for neuroprotection. *BMC Neurosci.*, **3**, 6.
85. Bacher,M., Deuster,O., Aljabari,B., Egensperger,R., Neff,F., Jessen,F., Popp,J., Noelker,C., Reese,J.P., Al-Abed,Y., *et al.* (2010) The role of macrophage migration inhibitory factor in Alzheimer's disease. *Mol. Med.*, **16**, 116–121.
86. David,J.R. (1966) Delayed hypersensitivity in vitro: its mediation by cell-free substances formed by lymphoid cell-antigen interaction. *Proc. Natl. Acad. Sci. U.S.A.*, **56**, 72–77.
87. Bloom,B.R. and Bennett,B. (1966) Mechanism of a reaction in vitro associated with delayed-type hypersensitivity. *Science*, **153**, 80–82.
88. Cox,G.M., Kithcart,A.P., Pitt,D., Guan,Z., Alexander,J., Williams,J.L., Shawler,T., Dagia,N.M., Popovich,P.G., Satoskar,A.R., *et al.* (2013) Macrophage migration inhibitory factor potentiates autoimmune-mediated neuroinflammation. *J. Immunol.*, **191**, 1043–1054.
89. Bernhagen,J., Krohn,R., Lue,H., Gregory,J.L., Zernecke,A., Koenen,R.R., Dewor,M., Georgiev,I., Schober,A., Leng,L., *et al.* (2007) MIF is a noncognate ligand of CXC chemokine receptors in inflammatory and atherogenic cell recruitment. *Nat. Med.*, **13**, 587–596.
90. Oliveros,G., Wallace,C.H., Chaudry,O., Liu,Q., Qiu,Y., Xie,L., Rockwell,P., Figueiredo-Pereira,M.E. and Serrano,P.A. (2023) Repurposing ibudilast to mitigate Alzheimer's disease by targeting inflammation. *Brain*, **146**, 898–911.
91. Angelopoulou,E., Pyrgelis,E.-S. and Piperi,C. (2022) Emerging potential of the phosphodiesterase (PDE) inhibitor Ibudilast for neurodegenerative diseases: an update on preclinical and clinical evidence. *Molecules*, **27**, 8448.

92. Wang,H., Mei,Z.l., Zhong,K.L., Hu,M., Long,Y., Miao,M.X., Li,N., Yan,T.H. and Hong,H. (2014) Pretreatment with antiasthmatic drug ibudilast ameliorates Aβ1–42-induced memory impairment and neurotoxicity in mice. *Pharmacol. Biochem. Behav.*, **124**, 373–379.
93. Fukui,R., Saitoh,S.-I., Kanno,A., Onji,M., Shibata,T., Ito,A., Onji,M., Matsumoto,M., Akira,S., Yoshida,N., *et al.* (2011) Unc93B1 restricts systemic lethal inflammation by orchestrating toll-like receptor 7 and 9 trafficking. *Immunity*, **35**, 69–81.
94. Lee,B.L., Moon,J.E., Shu,J.H., Yuan,L., Newman,Z.R., Schekman,R. and Barton,G.M. (2013) UNC93B1 mediates differential trafficking of endosomal TLRs. *eLife*, **2**, e00291.
95. Pelka,K., Bertheloot,D., Reimer,E., Phulphagar,K., Schmidt,S.V., Christ,A., Stahl,R., Watson,N., Miyake,K., Hacohen,N., *et al.* (2018) The chaperone UNC93B1 regulates toll-like receptor stability independently of endosomal TLR transport. *Immunity*, **48**, 911–922.
96. Klammer,M.G., Dzaye,O., Wallach,T., Krüger,C., Gaessler,D., Buonfiglioli,A., Derkow,K., Kettenmann,H., Brinkmann,M.M. and Lehnardt,S. (2021) UNC93B1 is widely expressed in the murine CNS andis required for neuroinflammation and neuronal injury induced by MicroRNA let-7b. *Front. Immunol.*, **12**, 715774.
97. Rath,S., Sharma,R., Gupta,R., Ast,T., Chan,C., Durham,T.J., Goodman,R.P., Grabarek,Z., Haas,M.E., Hung,W.H.W., *et al.* (2021) MitoCarta3.0: an updated mitochondrial proteome now with sub-organelle localization and pathway annotations. *Nucleic Acids Res.*, **49**, D1541–D1547.
98. Wu,M., Neilson,A., Swift,A.L., Moran,R., Tamagnine,J., Parslow,D., Armistead,S., Lemire,K., Orrell,J., Teich,J., *et al.* (2007) Multiparameter metabolic analysis reveals a close link between attenuated mitochondrial bioenergetic function and enhanced glycolysis dependency in human tumor cells. *Am. J. Physiol. Cell Physiol.*, **292**, C125–C136.
99. Plitzko,B. and Loesgen,S. (2018) Measurement of oxygen consumption rate (OCR) and extracellular acidification rate (ECAR) in culture cells for assessment of the energy metabolism. *Bio Protoc*, **8**, e2850.
100. Sola-Penna,M., Da Silva,D., Coelho,W.S., Marinho-Carvalho,M.M. and Zancan,P. (2010) Regulation of mammalian muscle type 6-phosphofructo-1-kinase and its implication for the control of the metabolism. *IUBMB Life*, **62**, 791–796.
101. Yi,W., Clark,P.M., Mason,D.E., Keenan,M.C., Hill,C., Goddard,W.A., Peters,E.C., Driggers,E.M. and Hsieh-Wilson,L.C. (2012) Phosphofructokinase 1 glycosylation regulates cell growth and metabolism. *Science*, **337**, 975–980.
102. Kabiraj,P., Grund,E.M., Clarkson,B.D.S., Johnson,R.K., LaFrance-Corey,R.G., Lucchinetti,C.F. and Howe,C.L. (2022) Teriflunomide shifts the astrocytic bioenergetic profile from oxidative metabolism to glycolysis and attenuates TNFα-induced inflammatory responses. *Sci. Rep.*, **12**, 3049.
103. Motori,E., Puyal,J., Toni,N., Ghanem,A., Angeloni,C., Malaguti,M., Cantelli-Forti,G., Berninger,B., Conzelmann,K.-K., Götz,M., *et al.* (2013) Inflammation-induced alteration of astrocyte mitochondrial dynamics requires autophagy for mitochondrial network maintenance. *Cell Metab.*, **18**, 844–859.
104. Robb,J.L., Hammad,N.A., Weightman Potter,P.G., Chilton,J.K., Beall,C. and Ellacott,K.L.J. (2020) The metabolic response to inflammation in astrocytes is regulated by nuclear factor-kappa B signaling. *Glia*, **68**, 2246–2263.
105. Inoue,F. and Ahituv,N. (2015) Decoding enhancers using massively parallel reporter assays. *Genomics*, **106**, 159–164.
106. Korkmaz,G., Lopes,R., Ugalde,A.P., Nevedomskaya,E., Han,R., Myacheva,K., Zwart,W., Elkon,R. and Agami,R. (2016) Functional genetic screens for enhancer elements in the human genome using CRISPR-Cas9. *Nat. Biotechnol.*, **34**, 192–198.
107. Li,K., Liu,Y., Cao,H., Zhang,Y., Gu,Z., Liu,X., Yu,A., Kaphle,P., Dickerson,K.E., Ni,M., *et al.* (2020) Interrogation of enhancer function by enhancer-targeting CRISPR epigenetic editing. *Nat. Commun.*, **11**, 485.
108. Corradin,O. and Scacheri,P.C. (2014) Enhancer variants: evaluating functions in common disease. *Genome Med.*, **6**, 85.
109. Sakabe,N.J., Savic,D. and Nobrega,M.A. (2012) Transcriptional enhancers in development and disease. *Genome Biol.*, **13**, 238.
110. Smith,E. and Shilatifard,A. (2014) Enhancer biology and enhanceropathies. *Nat. Struct. Mol. Biol.*, **21**, 210–219.
111. Zaugg,J.B., Sahlén,P., Andersson,R., Alberich-Jorda,M., de Laat,W., Deplancke,B., Ferrer,J., Mandrup,S., Natoli,G., Plewczynski,D., *et al.* (2022) Current challenges in understanding the role of enhancers in disease. *Nat. Struct. Mol. Biol.*, **29**, 1148–1158.
112. Finkel,R.S., Mercuri,E., Darras,B.T., Connolly,A.M., Kuntz,N.L., Kirschner,J., Chiriboga,C.A., Saito,K., Servais,L., Tizzano,E., *et al.*2017) Nusinersen versus Sham control in infantile-onset spinal muscular atrophy. *N. Engl. J. Med.*, **377**, 1723–1732.
113. Acsadi,G., Crawford,T.O., Müller-Felber,W., Shieh,P.B., Richardson,R., Natarajan,N., Castro,D., Ramirez-Schrempp,D., Gambino,G., Sun,P., *et al.* (2021) Safety and efficacy of nusinersen in spinal muscular atrophy: the EMBRACE study. *Muscle Nerve*, **63**, 668–677.
114. Finkel,R.S., Chiriboga,C.A., Vajsar,J., Day,J.W., Montes,J., De Vivo,D.C., Bishop,K.M., Foster,R., Liu,Y., Ramirez-Schrempp,D., *et al.* (2021) Treatment of infantile-onset spinal muscular atrophy with nusinersen: final report of a phase 2, open-label, multicentre, dose-escalation study. *Lancet Child Adolesc. Health*, **5**, 491–500.
115. Frangoul,H., Altshuler,D., Cappellini,M.D., Chen,Y.-S., Domm,J., Eustace,B.K., Foell,J., de la Fuente,J., Grupp,S., Handgretinger,R., *et al.*2021) CRISPR-Cas9 gene editing for Sickle cell disease and β-thalassemia. *N. Engl. J. Med.*, **384**, 252–260.
116. Liddelow,S.A., Guttenplan,K.A., Clarke,L.E., Bennett,F.C., Bohlen,C.J., Schirmer,L., Bennett,M.L., Münch,A.E., Chung,W.-S., Peterson,T.C., *et al.* (2017) Neurotoxic reactive astrocytes are induced by activated microglia. *Nature*, **541**, 481–487.
117. Guttenplan,K.A., Weigel,M.K., Prakash,P., Wijewardhane,P.R., Hasel,P., Rufen-Blanchette,U., Münch,A.E., Blum,J.A., Fine,J., Neal,M.C., *et al.* (2021) Neurotoxic reactive astrocytes induce cell death via saturated lipids. *Nature*, **599**, 102–107.
118. Lovén,J., Hoke,H.A., Lin,C.Y., Lau,A., Orlando,D.A., Vakoc,C.R., Bradner,J.E., Lee,T.I. and Young,R.A. (2013) Selective inhibition of tumor oncogenes by disruption of super-enhancers. *Cell*, **153**, 320–334.
119. Kanno,T., Kanno,Y., LeRoy,G., Campos,E., Sun,H.-W., Brooks,S.R., Vahedi,G., Heightman,T.D., Garcia,B.A., Reinberg,D., *et al.* (2014) BRD4 assists elongation of both coding and enhancer RNAs by interacting with acetylated histones. *Nat. Struct. Mol. Biol.*, **21**, 1047–1057.
120. Takeuchi,T., Yamazaki,Y., Katoh-Fukui,Y., Tsuchiya,R., Kondo,S., Motoyama,J. and Higashinakagawa,T. (1995) Gene trap capture of a novel mouse gene, jumonji, required for neural tube formation. *Genes Dev.*, **9**, 1211–1222.
121. Takeuchi,T., Watanabe,Y., Takano-Shimizu,T. and Kondo,S. (2006) Roles of jumonji and jumonji family genes in chromatin regulation and development. *Dev. Dyn.*, **235**, 2449–2459.
122. Gorbovytska,V., Kim,S.-K., Kuybu,F., Götze,M., Um,D., Kang,K., Pittroff,A., Brennecke,T., Schneider,L.-M., Leitner,A., *et al.* (2022) Enhancer RNAs stimulate Pol II pause release by harnessing multivalent interactions to NELF. *Nat. Commun.*, **13**, 2429.
123. Schaukowitch,K., Joo,J.-Y., Liu,X., Watts,J.K., Martinez,C. and Kim,T.-K. (2014) Enhancer RNA facilitates NELF release from immediate early genes. *Mol. Cell*, **56**, 29–42.

Received: May 1, 2024. **Revised:** July 26, 2024. **Editorial Decision:** July 27, 2024. **Accepted:** August 1, 2024
Published by Oxford University Press on behalf of Nucleic Acids Research 2024.